Canadian Mineralogist
Vol. 15, pp. 321-338 (1977)

SYNTHESIS AND CRYSTAL-STRUCTURE REFINEMENT OF TRANSITION-METAL ORTHOPYROXENES I: ORTHOENSTATITE AND (Mg, Mn, Co) ORTHOPYROXENE

F. C. HAWTHORNE

Department of Earth Sciences, University of Manitoba, Winnipeg, Man.

JUN ITO

James Franck Institute, University of Chicago, Chicago, Illinois 60637

ABSTRACT

Large, high-quality crystals of orthoenstatite and transition-metal orthopyroxenes have been synthesized using lithium vanadomolybdate as a high-temperature solvent. Optimum synthesis conditions in the system Li_2O-MoO_3-V_2O_5-MgO-SiO_2 have been defined; under these conditions, crystals average $5\times2\times1$ mm, with the largest exceeding 10 mm in length. Crystals are euhedral and lack cleavage, parting, or observable defects; inclusions of flux components are rare. Two factors involved in producing a high yield of good-quality crystals are: (i) the temperature of equilibration prior to cooling should not exceed that of the ortho → proto inversion; (ii) the rate of cooling must not exceed 1.5°C/hour as more rapid cooling promotes the crystallization of metastable forsterite and/or protoenstatite.

Three-dimensional counter-collected single-crystal X-ray data were used to refine the crystal structures of orthoenstatite [*a* 18.216(2), *b* 8.813(1), *c* 5.179(1)Å] and a synthetic orthopyroxene of composition $Mg_{1.562}Mn_{0.175}Co_{0.263}Si_2O_6$ [*a* 18.246(3), *b* 8.839(2), *c* 5.196(1)Å] in the space group *Pbca*. The final *R*-indices for 1223 and 1129 observed reflections are 3.3% and 4.1%, respectively. The results for orthoenstatite differ only slightly from those of Morimoto & Koto (1969), but are more precise. The Mg/transition-metal site-occupancies of the (Mg,Mn,Co) orthopyroxene were derived by constrained site-population refinement of the X-ray data.

Mean bond-length–constituent-cation radius relationships for synthetic orthopyroxenes are extremely non-linear. Octahedral bond-length distortions are large and have a considerable effect on mean bond lengths. Bond-length distortion is not a linear function of constituent-cation radius, and this results in non-linear bond-length–cation-radius relationships for both octahedral sites. For natural orthopyroxenes, variation in bond-length distortion does not contribute significantly to changes in $\langle M1\text{-O}\rangle$. The $\langle M1\text{-O}\rangle$-$r_{M1}$ relationship suggests that minor trivalent cations are enriched in incoherently-diffracting microstructures and do not completely contribute to variations in $\langle M1\text{-O}\rangle$; this is supported by the $\langle Si\text{-O}\rangle$-tetrahedral Al relationship. For the *M*2 octahedron, the variations in both $\langle M2\text{-O}\rangle$ and *M*2 bond-length distortion are non-linear with constituent-cation radius; in addition, the constituent-cation radius cannot be uniquely defined as Ca may be preferentially concentrated in incoherently-diffracting microstructures. The degree to which each of these factors affects the $\langle M2\text{-O}\rangle$-$r_{M2}$ relationship cannot be assessed until additional data on synthetic (Mg,Fe) orthopyroxenes are available.

In (Mg,Mn,Co) orthopyroxene, consideration of the mean octahedral bond lengths, together with the site-refinement results, indicates the following site-populations: $M1=0.904(4)Mg + 0.065Co^{2+} + 0.031Mn^{2+}$; $M2=0.658Mg + 0.198Co^{2+} + 0.144Mn^{2+}$. Structural distortion in the orthopyroxene structure is dominated by the bond-strength requirements of the anions; superimposed upon this is relaxation across shared polyhedral elements in order to reduce cation-cation repulsion. These distortions are operative under the general constraint that the *c*-axis repeats of the octahedral and both tetrahedral chains in the structure must be identical.

SOMMAIRE

De grands cristaux d'orthoenstatite et d'orthopyroxènes de métaux de transition, de très bonne qualité, ont été synthétisés à haute température à l'aide du vanadomolybdate de lithium utilisé comme solvant. Les meilleures conditions de synthèse dans le système Li_2O-MoO_3-V_2O_5-MgO-SiO_2 ont été définies; dans ces conditions, les cristaux mesurent en moyenne $5\times2\times1$ mm et le plus grand dépasse 10 mm de longueur. Les cristaux sont automorphes sans clivage, plan de séparation ou autres défauts observables. Les inclusions de fondant sont rares. Les deux facteurs qui conditionnent le rendement élevé de cristaux de bonne qualité sont: (1) la température d'équilibration avant le refroidissement ne devrait pas excéder celle de l'inversion ortho → proto; (2) le taux de refroidissement ne doit excéder 1.5°C par heure, car un refroidissement plus rapide provoque la cristallisation de forstérite et/ou de protoenstatite métastables.

Les données tridimensionnelles recueillies sur monocristal par diffraction des rayons X avec compteur ont été utilisées pour affiner les structures cristallines de l'orthoenstatite [*a* 18.216(2), *b* 8.813(1),

c 5.179(1)Å] et d'un orthopyroxène synthétique $Mg_{1.562}Mn_{0.175}Co_{0.263}Si_2O_6$ [*a* 18.246(3), *b* 8.839(2), *c* 5.196(1)Å] dans le groupe spatial *Pbca*. Les derniers indices *R* de 3.3% et de 4.1% ont été obtenus respectivement pour 1223 et 1129 réflexions observées. Les résultats obtenus pour l'orthoenstatite ne diffèrent que légèrement de ceux obtenus par Morimoto & Koto (1969), mais sont plus exacts. L'occupation des sites Mg/métal de transition dans l'orthopyroxène (Mg,Mn,Co) a été déterminée par un affinement restreint aux variables des sites.

Les relations entre la longueur moyenne des liaisons et le rayon des cations des orthopyroxènes synthétiques sont très fortement non linéaires. Les distortions des liaisons octaédriques sont grandes et affectent considérablement la longueur moyenne des liaisons. Le fait que la distortion des liaisons n'est pas linéairement reliée au rayon du cation donne lieu à des relations non linéaires entre la longueur des liaisons et le rayon du cation pour les deux sites octaédriques. Dans le cas des orthopyroxènes naturels, la variation dans la distortion des longueurs de liaison n'influence pas beaucoup les changements en $<M1\text{-}O>$. Les relations $<M1\text{-}O>$-r_{M1} suggèrent que les cations mineurs trivalents s'enrichissent dans des micro-structures à diffraction incohérente et ne contribuent pas entièrement aux variations de $<M1\text{-}O>$; ceci est mis en évidence par les relations $<SiB\text{-}O>$-Al tétraédrique. Dans l'octaèdre *M2*, les variations dans la distortion des longueurs de liaison $<M2\text{-}O>$ et de *M2* en fonction du rayon du cation sont non-linéaires, de plus, le rayon du cation ne peut être défini uniquement, Ca pouvant être concentré de façon préférentielle dans des micro-structures à diffraction incohérente. Le degré avec lequel chacun de ces facteurs affecte les relations $<M2\text{-}O>$-r_{M2} ne peut être évalué tant qu'on ne possède pas plus d'information sur les orthopyroxènes (Mg,Fe) synthétiques.

Si on tient compte des longueurs moyennes des liaisons octaédriques ainsi que des résultats d'affinement des sites dans l'orthopyroxène (Mg,Mn,Co), on trouve les populations de site suivantes: $M1 = 0.904(4)Mg + 0.065Co^{2+} + 0.031Mn^{2+}$; $M2 = 0.658Mg + 0.198Co^{2+} + 0.144Mn^{2+}$. La distorsion structurale de l'orthopyroxène est dominée par les exigences des anions sur la force des liaisons; s'ajoute à ceci une relaxation entre les éléments en commun des polyèdres afin de réduire la répulsion cation-cation. Ces distorsions se produisent sous la condition générale qui veut que les périodes *c* de la chaîne octaédrique et des deux chaînes tétraédriques de la structure soient identiques.

(Traduit par la Rédaction)

Introduction

Orthopyroxenes are common constituents of a wide variety of plutonic, volcanic, and high-grade metamorphic rocks and have been extensively investigated by mineralogists and petrologists because of their potentially useful application as geothermometers and geobarometers. The orthopyroxene structure contains two non-equivalent octahedral sites and accurate site-populations may be obtained by least-squares refinement of X-ray or Mössbauer (Fe^{2+}) data. It was first shown by Ghose (1965a) that Fe^{2+} was strongly ordered into the *M2* site of a metamorphic bronzite. Subsequent work both using X-ray diffraction (Burnham *et al.* 1971; Smyth 1973; Takeda 1971, 1972a,b; Miyamoto 1974) and Mössbauer spectroscopy (Evans *et al.* 1967; Bancroft *et al.* 1967; Ghose & Hafner 1967; Virgo & Hafner 1970) has confirmed the strong ordering of Fe^{2+} into the *M2* site in natural orthopyroxenes and indicated that the observed cation-ordering is a function of the temperature of equilibration. The latter has been confirmed by heating experiments in conjunction with both Mössbauer spectroscopy (Virgo & Hafner 1969) and X-ray diffraction (Smyth 1973). Interest has also focused on the intercrystalline distribution of cations between orthopyroxene and various coexisting minerals (Kretz 1961, 1963; Matsui & Banno 1970; Medaris 1969; Nishizawa & Akimoto 1973; Maxey & Vogel 1974; Wood & Banno 1973) and attempts have been made (Grover & Orville 1969; Blander 1970) to allow for the occurrence of two distinct octahedral sites in the orthopyroxene structure. These studies have generally been unsatisfactory in that the non-ideality of the mixing is not well-characterized and ideal mixing is generally assumed. However, this has been shown not to be the case in orthopyroxene where Mg-Fe^{2+} mixing departs considerably from an ideal model (Saxena & Ghose 1971).

The crystal-chemical factors that govern cation distribution in minerals are not well-understood. Various cationic properties such as ionic radius, formal charge, electronegativity, and polarizability have been used to forecast site-preferences in minerals (e.g. Ghose 1962, 1965b). This is further complicated for transition-metal cations where crystal-field stabilization energies become important (Burns 1970a,b). Most workers have also recognized that the occurrence of additional cations in a mineral will modify the site-occupancies of the major components (e.g. Blander 1972; Snellenburg 1975). This seems to be important in the orthopyroxenes where Ca occupies the *M2* site, selectively displacing Fe^{2+} and causing increased disorder (Virgo & Hafner 1970).

In order to obtain a better understanding of cation-ordering patterns in minerals, the study of synthetic analogues has many advantages over similar studies of natural minerals. There are no minor elements present in sufficient amounts to significantly affect the cation-order-

ing pattern of the major constituents. In addition, a wide variety of compounds may be examined, many of which do not occur in nature. The results presented here constitute a preliminary investigation to find a suitable high-temperature solvent for crystal growth in air, together with the characterization of the resultant crystals by X-ray diffraction.

The crystal structure of orthopyroxene (enstatite) was first determined by Warren & Modell (1930); revised atomic coordinates based on 2-dimensional Fourier syntheses were given by Lindemann (1961). The first 3-D refinement of an orthopyroxene was of a bronzite (Ghose 1965a), where it was first demonstrated that considerable Mg-Fe^{2+} ordering occurs in the orthopyroxene structure. Morimoto & Koto (1969), Burnham (1967) and Sueno *et al.* (1976) presented refinements of orthoenstatite and synthetic orthoferrosilite. Further refinements of natural orthopyroxenes have been given by Burnham *et al.* (1971), Takeda (1971, 1972a,b), Miyamoto *et al.* (1975), Kosoi *et al.* (1974), Miyamoto (1974), Smyth (1973), Takeda & Ridley (1972), and Ghose & Wan (1973), and preliminary results for a series of synthetic transition-metal orthopyroxenes were given by Ghose *et al.* (1974, 1975, 1976).

Crystal Synthesis

The high-temperature solvent lithium vanadomolybdate (Li_2O=51.2, MoO_3=42.8, V_2O_5=6.0 mol. %) was used successfully by Grandin de L'Eprevier (1972) in the growth of forsterite crystals, and seemed to be a promising flux for the growth of orthopyroxene (Ito 1975). As orthoenstatite is stable only between 650 and 950°C, the synthesis was attempted by equilibration and slow cooling within this temperature range. Details of the charge compositions used for the crystals synthesized in this study are given in Table 1. The charge was heated to 930°C in a muffle furnace and left for 14 days to achieve complete equilibration*. The resultant melt was cooled slowly to 650°C and then quenched to room temperature. The water-soluble flux components were then removed by soaking in hot distilled water and washing. Large single crystals of orthoenstatite were produced, together with minor flaky $Li_2Si_2O_5$ (Donnay & Donnay 1953). White, translucent, low clinoenstatite was occasionally present in very small amounts. The crystals average 5×2×1 mm, with the largest exceeding 10 mm in length, and were elongate along *c*. The most prominent forms are the {210} prism and the {100} and {010} pinacoids. The crystals are either singly or doubly terminated and characteristically lack cleavage, parting, or observable defects; inclusions are rare.

TABLE 1. CRYSTAL AND SYNTHESIS DATA

	Orthoenstatite			
a(Å)	18.214(4)	18.216(2)	18.210(10)	18.225(1)
b(Å)	8.818(2)	8.813(1)	8.812(5)	8.815(1)
c(Å)	5.177(2)	5.179(1)	5.178(4)	5.175(1)
ref.	1a	1b	2	3

	Low clinoenstatite		(Mg,Mn,Co) orthopyroxene
a(Å)	9.609(2)	9.607(1)	18.246(3)
b(Å)	8.814(2)	8.815(1)	8.839(2)
c(Å)	5.175(2)	5.169(1)	5.196(1)
β(°)	108.37(2)	108.34(1)	90
ref.	1a	3	1b

Orthoenstatite[4]				Mg-Mn-Co Orthopyroxene			
Charge	Comp.	Analysis		Charge	Comp.	Analysis	
SiO_2	0.906gm	SiO_2	60.0	SiO_2	2.095gm	SiO_2	-
MgO	0.606	MoO_3	-	MgO	0.586	MoO_3	0.03
$CoCO_3$	-	V_2O_5	0.27	$CoCO_3$	0.849	V_2O_5	0.29
$MnCO_3$	-	MgO	40.3	$MnCO_3$	0.900	MgO	28.6
Li_2CO_3	7.35	MnO	-	Li_2CO_3	14.70	MnO	5.65
MoO_3	11.70	CoO	-	MoO_3	23.40	CoO	8.95
V_2O_5	2.08	Li_2O	0.17	V_2O_3	4.16	Li_2O	0.22
Equilibration temperature (°C)	930			1020			
Formula unit	$Mg_2Si_2O_6$			$Mg_{1.562}Mn_{0.175}Co_{0.263}Si_2O_6$			
Space Group	*Pbca*			*Pbca*			
Z	8			8			
Rad/Monochromator				Mo/Graphite			Mo/Graphite
No. of non-equivalent observed reflections				1223			1129
Final R-factor				3.3%			4.1%
Final R_w-factor				4.1%			5.5%

$$R\ (\%) = \Sigma\ (\ |F_{obs}| - |F_{calc}|\ ) \ /\ \Sigma\ |F_{obs}|$$

$$R_w\ (\%) = (\Sigma w(|F_{obs}| - |F_{calc}|)^2\ /\ \Sigma w F_{obs}^2)^{\frac{1}{2}},\ w = 1$$

Temperature factor form: $\exp\ [-\ \sum_{i=1}^{3}\ \sum_{j=1}^{3}\ h_i h_j\ \beta_{ij}]$

1. This study: a - powder data; b - single-crystal data
2. Morimoto & Koto (1969)
3. Stephenson *et al.* (1966).
4. If Li_2SiO_3 is used, Li_2SiO_3 = 1.39gm & Li_2CO_3 = 6.24gm.

Higher equilibration temperatures were tried in the synthesis of orthoenstatite, together with variations in the rate of cooling. This generally led to the formation of large amounts of clinoenstatite (presumably formed by a martensitic transformation from protoenstatite — Smyth 1974) together with orthoenstatite and some forsterite. The solvent-to-charge ratio was also varied, but this invariably led to less satisfactory results; increasing this ratio resulted in slightly yellowish crystals, suggesting a substitution of solvent components into the orthoenstatite structure, possibly by the coupled substitution $Li^+ + V^{5+} \rightleftharpoons Mg^{2+} + Si^{4+}$. Total exclusion of V_2O_5 from the system gave colorless orthoenstatite, but the size and yield of the crystals were considerably reduced.

*We have since found that the lengthy equilibration time can be shortened by a factor of three by using Li_2SiO_3 instead of H_2SiO_3.

EXPERIMENTAL

Chemical analyses were performed by electron microprobe and atomic absorption, and the results are given in Table 1. The major impurities found in the bulk sample were Li_2O and V_2O_5, but the probe analysis showed that vanadium is concentrated at the core of the crystal and is below the limit of detection (0.1 wt. %) at the rim. Consequently, care was taken to select a fragment from the edge of a large crystal for the collection of the single-crystal X-ray intensity data. Unit-cell contents were calculated on the basis of two octahedral cations per formula unit, ignoring any Li and V in the analysis.

Single-crystal X-ray precession photographs confirmed the space group *Pbca* established by many previous studies (e.g. Morimoto & Koto 1969). Unit-cell dimensions for the bulk orthoenstatite sample and low clinoenstatite were refined from X-ray powder-diffraction data using Cu$K\alpha_1$ radiation with a Si standard. Cell dimensions were also determined for both orthopyroxene samples by least-squares refinement of 15 reflections automatically aligned on a 4-circle diffractometer. These values are compared (Table 1) with values obtained previously by Stephenson *et al.* (1966) and Morimoto & Koto (1969).

The crystals used in the collection of the intensity data were irregular, equidimensional fragments of ~0.1 mm diameter; they showed sharp extinction under the polarizing microscope and no inclusions were visible. The crystals were mounted on a Syntex $P\bar{1}$ automatic diffractometer operating in the θ-2θ scan mode with variable scan rates from 2.0-24.0 0°/min., depending on the peak count through an angle of 2° and the α_1–α_2 separation. Graphite - monochromated Mo$K\alpha$ radiation (λ=0.71069Å) was used, and background counts were made at the beginning and end of each scan. One standard reflection was monitored every 50 reflections to check for crystal misorientation; no significant change was noted during data collection. Intensity data were collected over one asymmetric unit out to a 2θ value of 65°. The data were corrected for Lorentz, polarization, and background effects, but no absorption corrections were performed as preliminary calculations showed them to be negligible for these crystals. A reflection was considered as observed if its magnitude exceeded that of three standard deviations based on counting statistics. Application of this procedure resulted in 1797 (1798) reflections for orthoenstatite (Mg, Mn, Co opx.) of which 1231 (1135) were considered as observed.

REFINEMENT

Scattering factors for neutral atoms were taken from Cromer & Mann (1968) with anomalous dispersion corrections from Cromer & Liberman (1970). The final atomic parameters of orthoenstatite (Morimoto & Koto 1969) were used as input to the least-squares program RFINE (Finger 1969a). For orthoenstatite, full-matrix refinement of all variables for an isotropic thermal model resulted in convergence at R- and R_w-indices (see Table 1) of 4.8% and 5.1% respectively (observed data only). Temperature factors were converted to anisotropic of the form given in Table 1, and a correction was made for (isotropic) extinction (Zachariasen 1968) with the extinction coefficient included as a variable in the refinement. Refinement of all variables resulted in convergence at R-indices of 3.3% (observed) and 4.1% (all data) and R_w-indices of 3.6% (observed) and 4.1% (all data). For the (Mn,Co,Mg) orthopyroxene, the refinement procedure was similar except that the site-populations were also considered as variable. As Mn ($Z = 25$) and Co ($Z = 27$) have similar scattering factors, they were treated as one scattering species represented by the scattering curve for Fe ($Z = 26$); the 'Fe' site-distribution was refined using the known bulk composition as a constraint in the refinement (Finger 1969b). Using isotropic temperature factors, refinement of all variables resulted in convergence at R- and R_w-indices of 5.2% and 5.9% respectively (observed data only). When anisotropic temperature factors were used, the refinement converged at R-indices of 4.0% (observed) and 5.3% (all data), and R_w-indices of 4.7% (observed) and 5.6% (all data). Observed and calculated structure factors are listed in Table 2*, atomic coordinates and equivalent isotropic temperature factors in Table 3, and anisotropic temperature factor coefficients in Table 4. Interatomic distances and angles, and the magnitudes and orientations of the principal axes of the thermal ellipsoids, were calculated with the program ERRORS (L. W. Finger, pers. comm.) and are presented in Tables 5 and 6 respectively. Stereographic representations of the orientations of the principal axes of the thermal ellipsoids are given in Figures 1 and 2, where they are compared with the values given by Burnham *et al.* (1971) for a natural orthopyroxene. Fig-

*Table 2 may be obtained, at a nominal charge, from the Depository of Unpublished Data, CISTI, National Research Council of Canada, Ottawa K1A 0S2.

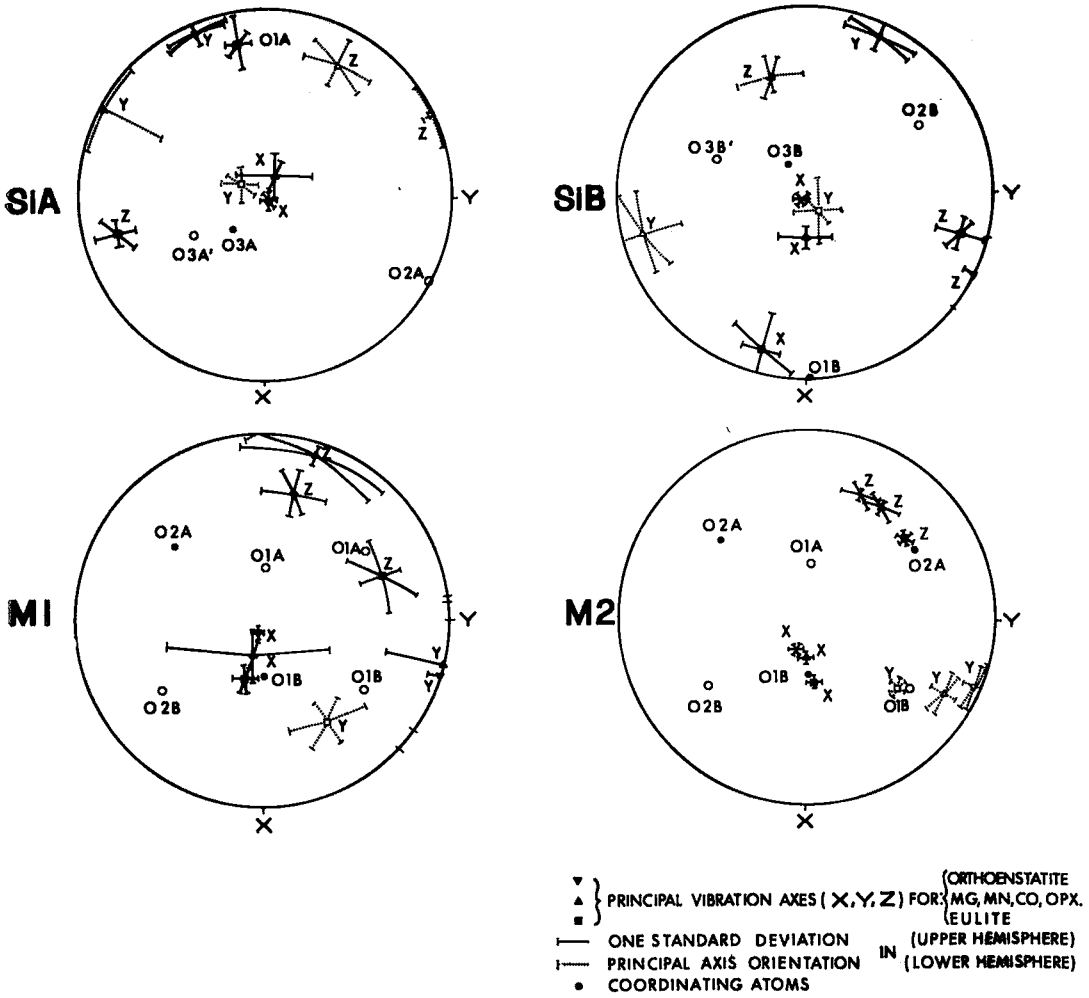

FIG. 1. Stereographic projection of the orientation of the principal axes of the thermal ellipsoids of the cations in orthoenstatite, (Mg,Mn,Co) orthopyroxene, and eulite (Burnham *et al.* 1971). The *X* and *Y* crystallographic axes are marked on the perimeter of the stereogram; the *Z* crystallographic axis is vertical.

ure 3 shows a (100) projection of the orthopyroxene structure that will be used in the following discussion.

DISCUSSION

Crystal growth

The results presented above indicate that lithium vanadomolybdate may be used successfully as a flux in the growth of high-quality orthopyroxene crystals. Small amounts of Li and V are incorporated into the structure and it is apparent that the elimination of these impurities is a major problem to pursue in future studies. Despite the flux-growing technique, vanadate and molybdate inclusions are rare. Two factors are involved in producing a high yield of good quality crystal: (i) the temperature for prolonged equilibration prior to cooling should not exceed that of ortho-proto inversion in order to avoid nucleation of protoenstatite upon cooling; (ii) the rate of cooling must not be greater than 1.5°C/hour, as more rapid cooling promotes the crystallization of metastable forsterite and/or protoenstatite which later inverts to low clinoenstatite.

Mean bond-length variations in orthopyroxenes

The crystal-structure refinement results given here for orthoenstatite are only slightly different from those given by Morimoto & Koto (1969), but they are considerably more precise.

This prompted a re-examination of structural variation in orthopyroxenes as there is considerable confusion in the literature concerning mean bond-length variation in the (Mg,Fe) orthopyroxenes. Morimoto & Koto (1969) proposed a linear variation in $<M1\text{-}O>$ bond length with increasing Fe^{2+} substitution into the $M1$ site. As this relationship did not agree with the experimental results of hypersthene (Ghose 1965), they suggested that the site-occupancies were

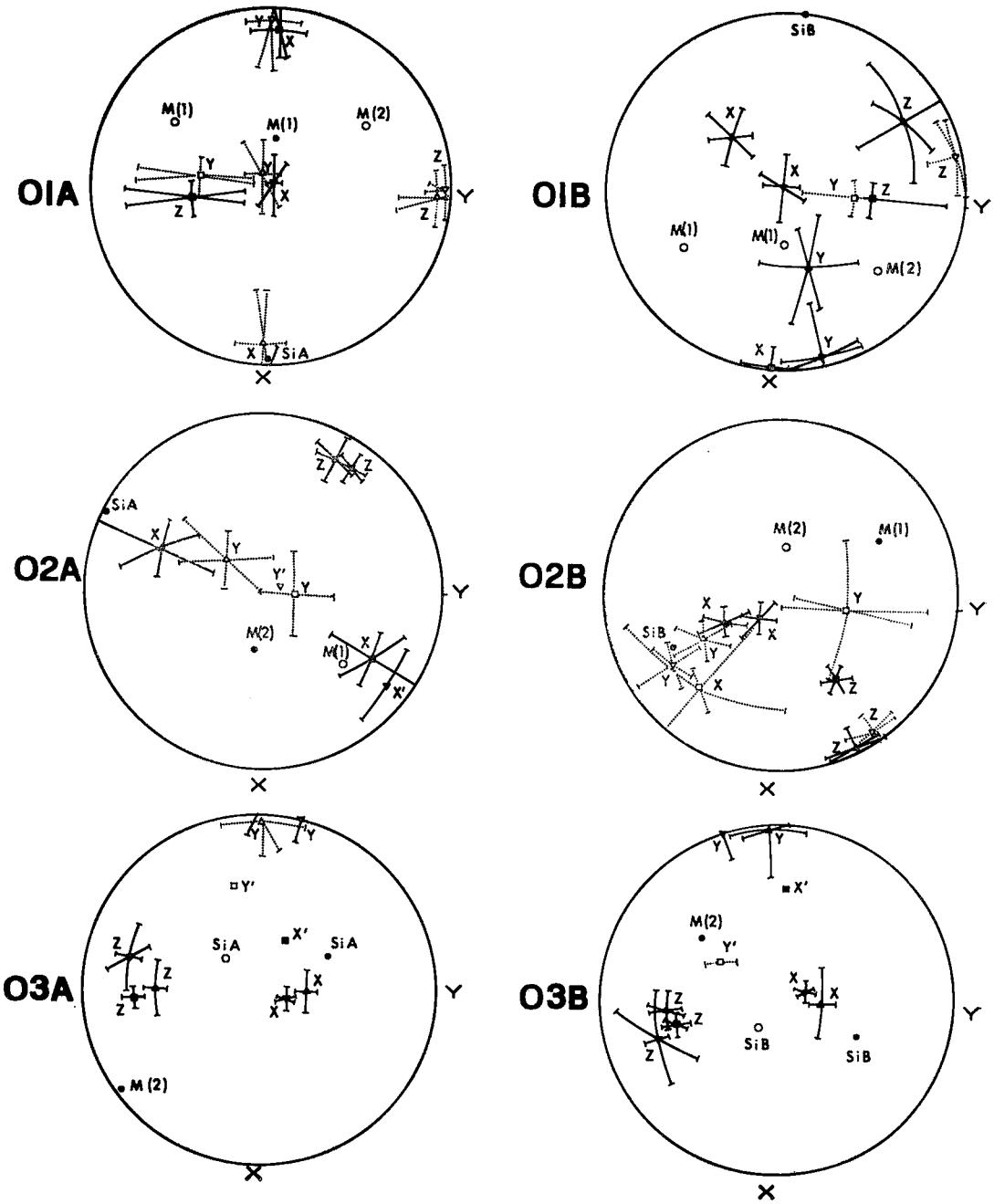

FIG. 2. Stereographic projection of the orientations of the principal axes of the thermal ellipsoids of the anions in orthoenstatite, (Mg,Mn,Co) orthopyroxene, and eulite. Legend as for Figure 1.

slightly in error. However, these site-occupancies were later confirmed by Mössbauer spectroscopy (Ghose & Hafner 1967). Morimoto & Koto (1969, footnote, p. 82) modified their view, proposing a non-linear relationship between <*M*-O> distances and Mg-Fe occupancy. Subsequently, Burnham *et al.* (1971) also proposed a non-linear variation for variations in <*M*1-O> bond length and Mg-Fe occupancy. More recently, Smyth (1973) proposed that this relationship was linear for the *M*1 site, and yet the value for orthoenstatite (Morimoto & Koto 1969) deviated significantly from this proposed relationship. Morimoto (1974) considered the relationships to be 'almost linear' whereas Kosoi *et al.* (1974) concluded that they were non-linear.

TABLE 3. FINAL ATOMIC POSITIONS AND EQUIVALENT ISOTROPIC TEMPERATURE FACTORS

	x	y	z	B equiv.
		Orthoenstatite		
M1	0.37580(5)	0.65386(9)	0.8660(2)	0.54(1)
M2	0.37682(5)	0.4870(1)	0.3587(2)	0.70(1)
S1A	0.27171(4)	0.34150(8)	0.0503(1)	0.43(1)
S1B	0.47356(3)	0.33730(8)	0.7982(1)	0.43(1)
O1A	0.18332(9)	0.3399(2)	0.0346(3)	0.54(2)
O2A	0.3110(1)	0.5024(2)	0.0434(4)	0.66(2)
O3A	0.3032(1)	0.2226(2)	-0.1678(4)	0.63(3)
O1B	0.5624(1)	0.3402(2)	0.7997(4)	0.56(2)
O2B	0.4328(1)	0.4832(2)	0.6890(4)	0.62(2)
O3B	0.4477(1)	0.1950(2)	0.6040(3)	0.59(3)
		Mg,Mn,Co Orthopyroxene		
M1	0.37562(6)	0.6541(1)	0.8704(1)	0.42(2)
M2	0.37712(5)	0.4851(1)	0.3636(2)	0.65(2)
S1A	0.27165(5)	0.3411(1)	0.0516(2)	0.46(2)
S1B	0.47381(5)	0.3371(1)	0.7960(2)	0.45(2)
O1A	0.1837(1)	0.3390(3)	0.0396(5)	0.60(4)
O2A	0.3106(1)	0.5019(3)	0.0468(5)	0.70(4)
O3A	0.3033(1)	0.2261(3)	-0.1714(6)	0.72(4)
O1B	0.5623(1)	0.3394(3)	0.7975(5)	0.60(4)
O2B	0.4337(1)	0.4846(3)	0.6935(5)	0.67(4)
O3B	0.4474(1)	0.1985(3)	0.5980(5)	0.65(4)

TABLE 4. ANISOTROPIC TEMPERATURE FACTORS (x 10^5)

	β_{11}	β_{22}	β_{33}	β_{12}	β_{13}	β_{23}
			Orthoenstatite			
M1	52(2)	209(9)	264(25)	-2(4)	-13(6)	7(13)
M2	65(2)	255(9)	424(27)	-7(4)	-45(7)	32(14)
S1A	37(2)	176(7)	252(19)	-5(3)	-2(4)	-5(9)
S1B	37(2)	173(7)	261(19)	5(3)	-4(4)	4(9)
O1A	36(4)	256(19)	327(52)	-1(7)	2(12)	-8(27)
O2A	59(4)	210(19)	503(56)	-30(8)	-14(13)	20(..)
O3A	53(4)	265(20)	324(54)	5(7)	-10(13)	-89(26)
O1B	42(4)	228(18)	388(52)	-8(7)	0(12)	10(28)
O2B	56(4)	224(19)	400(55)	23(7)	-16(13)	11(27)
O3B	52(4)	237(19)	313(55)	-3(7)	17(12)	-92(25)
			Mg,Mn,Co Orthopyroxene			
M1	37(3)	127(12)	350(37)	-4(4)	-15(7)	8(16)
M2	57(2)	238(10)	409(29)	-10(4)	-42(7)	16(13)
S1A	39(2)	150(10)	368(30)	-6(4)	9(7)	-9(15)
S1B	39(2)	147(10)	361(30)	4(4)	-22(7)	-7(15)
O1A	29(6)	268(29)	517(82)	1(11)	7(18)	-13(43)
O2A	67(7)	196(28)	539(80)	-32(12)	-8(19)	42(41)
O3A	54(6)	280(30)	509(84)	3(11)	0(20)	-156(41)
O1B	42(6)	200(26)	498(79)	-17(11)	12(19)	60(40)
O2B	67(7)	208(27)	441(80)	32(11)	-10(20)	61(41)
O3B	43(6)	276(28)	467(83)	-7(11)	7(19)	-141(40)

TABLE 5. SELECTED INTERATOMIC DISTANCES AND ANGLES

Orthoenstatite				(Mg,Mn,Co) Orthopyroxene			
S1A-O1A	1.612(2)Å	S1B-O1B	1.619(2)Å	S1A-O1A	1.606(3)Å	S1B-O1B	1.616(3)Å
S1A-O2A	1.588(2)	S1B-O2B	1.589(2)	S1A-O2A	1.588(3)	S1B-O2B	1.587(3)
S1A-O3A	1.644(2)	S1B-O3B	1.675(2)	S1A-O3A	1.646(3)	S1B-O3B	1.671(3)
S1A-O3A′	1.668(2)	S1B-O3B′	1.677(2)	S1A-O3A′	1.661(3)	S1B-O3B′	1.672(3)
<S1A-O>	1.628	<S1B-O>	1.640	<S1A-O>	1.625	<S1B-O>	1.637
M1-O1A	2.027(2)	M2-O1A	2.087(2)	M1-O1A	2.032(3)	M2-O1A	2.117(3)
M1-O1A	2.147(2)	M2-O2A	2.031(2)	M1-O1A	2.148(3)	M2-O2A	2.051(3)
M1-O2A	2.006(2)	M2-O3A	2.287(2)	M1-O2A	2.013(3)	M2-O3A	2.310(3)
M1-O1B	2.066(2)	M2-O1B	2.053(2)	M1-O1B	2.064(3)	M2-O1B	2.080(3)
M1-O1B	2.168(2)	M2-O2B	1.991(2)	M1-O1B	2.174(3)	M2-O2B	2.001(3)
M1-O2B	2.044(2)	M2-O3B	2.446(2)	M1-O2B	2.052(3)	M2-O3B	2.487(3)
<M1-O>	2.076	<M2-O>	2.149	<M1-O>	2.081	<M2-O>	2.174
O1A-O2A	2.731(2)	O1A-S1A-O2A	117.1(1)°	O1A-O2A	2.726(4)	O1A-S1A-O2A	117.2(2)°
O1A-O3A	2.634(2)	O1A-S1A-O3A	108.0(1)	O1A-O3A	2.638(4)	O1A-S1A-O3A	108.4(1)
O1A-O3A′	2.729(2)	O1A-S1A-O3A′	112.6(1)	O1A-O3A′	2.711(4)	O1A-S1A-O3A′	112.1(1)
O2A-O3A	2.701(3)	O2A-S1A-O3A	113.4(1)	O2A-O3A	2.691(4)	O2A-S1A-O3A	112.6(1)
O2A-O3A′	2.488(3)	O2A-S1A-O3A′	99.6(1)	O2A-O3A′	2.494(4)	O2A-S1A-O3A′	100.3(1)
O3A-O3A′	2.634(1)	O3A-S1A-O3A′	105.4(1)	O3A-O3A′	2.632(1)	O3A-S1A-O3A′	105.5(1)
<O-O>	2.653	<O-S1A-O>	109.4	<O-O>	2.649	<O-S1A-O>	109.4
O1B-O2B	2.738(2)	O1B-S1B-O2B	117.2(1)	O1B-O2B	2.729(4)	O1B-S1B-O2B	117.0(2)
O1B-O3B	2.651(2)	O1B-S1B-O3B	107.2(1)	O1B-O3B	2.651(4)	O1B-S1B-O3B	107.5(1)
O1B-O3B′	2.636(2)	O1B-S1B-O3B′	106.2(1)	O1B-O3B′	2.636(4)	O1B-S1B-O3B′	106.6(1)
O2B-O3B	2.592(3)	O2B-S1B-O3B	105.1(1)	O2B-O3B	2.589(4)	O2B-S1B-O3B	105.2(1)
O2B-O3B′	2.676(2)	O2B-S1B-O3B′	110.0(1)	O2B-O3B′	2.664(4)	O2B-S1B-O3B′	109.7(1)
O3B-O3B′	2.765(1)	O3B-S1B-O3B′	111.2(1)	O3B-O3B′	2.753(1)	O3B-S1B-O3B′	110.9(1)
<O-O>	2.676	<O-S1B-O>	109.5	<O-O>	2.670	<O-S1B-O>	109.5
O1A-O1A	3.036(2)	O1A-M1-O1A	93.3(1)	O1A-O1A	3.037(3)	O1A-M1-O1A	93.2(1)
O1A-O2A	2.981(3)	O1A-M1-O2A	95.3(1)	O1A-O2A	2.989(4)	O1A-M1-O2A	95.2(1)
O1A-O1B	2.847(2)	O1A-M1-O1B	85.4(1)	O1A-O1B	2.847(4)	O1A-M1-O1B	85.1(1)
O1A-O2B	2.746(3)	O1A-M1-O2B	84.8(1)	O1A-O2B	2.767(4)	O1A-M1-O2B	85.3(1)
O1B-O1A	2.847(2)	O1B-M1-O1A	85.0(1)	O1B-O1A	2.847(4)	O1B-M1-O1A	85.0(1)
O1B-O2A	2.812(2)	O1B-M1-O2A	87.4(1)	O1B-O2A	2.828(4)	O1B-M1-O2A	87.8(1)
O1B-O1B	3.038(2)	O1B-M1-O1B	91.7(1)	O1B-O1B	3.041(3)	O1B-M1-O1B	91.7(1)
O1B-O2B	3.073(3)	O1B-M1-O2B	96.8(1)	O1B-O2B	3.069(4)	O1B-M1-O2B	96.4(1)
O1A-O2A	2.977(3)	O1A-M1-O2A	91.5(1)	O1A-O2A	2.982(4)	O1A-M1-O2A	91.4(1)
O2A-O2B	2.885(3)	O2A-M1-O2B	90.8(1)	O2A-O2B	2.905(4)	O2A-M1-O2B	91.2(1)
O2B-O1B	3.168(3)	O2B-M1-O1B	96.7(1)	O2B-O1B	3.138(4)	O2B-M1-O1B	95.9(1)
O1B-O1A	2.802(2)	O1B-M1-O1A	81.0(1)	O1B-O1A	2.823(4)	O1B-M1-O1A	81.6(1)
<O-O>	2.933	<O-M1-O>	90.0	<O-O>	2.939	<O-M1-O>	90.0
O1A-O1B	2.802(2)	O1A-M2-O1B	85.2(1)	O1A-O1B	2.823(4)	O1A-M2-O1B	84.5(1)
O1A-O2B	2.746(2)	O1A-M2-O2B	84.6(1)	O1A-O2B	2.767(4)	O1A-Ma-O2B	86.4(1)
O1A-O2A	2.901(3)	O1A-M2-O2A	89.6(1)	O1A-O2A	2.923(4)	O1A-M2-O2A	89.1(1)
O1A-O3A	3.540(3)	O1A-M2-O3A	108.0(1)	O1A-O3A	3.601(4)	O1A-M2-O3A	108.8(1)
O1B-O2B	2.973(3)	O1B-M2-O2B	94.6(1)	O1B-O2B	2.989(4)	O1B-M2-O2B	94.2(1)
O1B-O2A	2.812(2)	O1B-M2-O2A	87.0(1)	O1B-O2A	2.828(4)	O1B-M2-O2A	86.4(1)
O1B-O3B	3.172(3)	O1B-M2-O3B	89.2(1)	O1B-O3B	3.225(4)	O1B-M2-O3B	89.4(1)
O2B-O3A	3.503(3)	O2B-M2-O3A	109.7(1)	O2B-O3A	3.567(4)	O2B-M2-O3A	111.5(1)
O2B-O3B	3.423(3)	O2B-M2-O3B	100.5(1)	O2B-O3B	3.501(4)	O2B-M2-O3B	102.0(1)
O2A-O3A	2.488(3)	O2A-M2-O3A	70.1(1)	O2A-O3A	2.494(4)	O2A-M2-O3A	69.5(1)
O2A-O3B	3.055(3)	O2A-M2-O3B	85.4(1)	O2A-O3B	3.073(4)	O2A-M2-O3B	84.7(1)
O3A-O3B	2.896(2)	O3A-M2-O3B	75.4(1)	O3A-O3B	2.900(4)	O3A-M2-O3B	74.3(1)
<O-O>	3.026	<O-M2-O>	90.0	<O-O>	3.058	<O-M2-O>	89.9
M1-M1	3.095(1)	S1A-O3A-S1A	134.2(1)	M1-M1	3.102(1)	S1A-O3A-S1A	135.2(2)
M1-M2	3.011(1)	S1B-O3B-S1B	128.0(1)	M1-M2	3.027(2)	S1B-O3B-S1B	129.3(2)
M1-M2	2.945(1)	O3A-O3A-O3A	158.9(1)	M1-M2	2.966(2)	O3A-O3A-O3A	161.6(2)
M1-M2	3.165(1)	O3B-O3B-O3B	139.0(1)	M1-M2	3.189(1)	O3B-O3B-O3B	141.4(2)
S1A-S1A	3.051(1)			S1A-S1A	3.057(1)		
S1B-S1B	3.012(1)			S1B-S1B	3.020(1)		

Most of the orthopyroxenes for which data are available are natural minerals and contain significant amounts of Ca,Ti,Cr,Mn,Fe^{3+} and Al. As the role of these cations in the structure is not well-characterized as yet, this discussion will initially be restricted to synthetic orthopyroxenes; the available data are listed in Table 7. Figure 4 shows the relationships between mean bond length and constituent ionic radius for the *M*1 and *M*2 sites. For both sites, the relationship is extremely non-linear. It has been shown that mean bond lengths in coordination polyhedra are sensitive to the degree of bond-length distortion* (Shannon & Calvo 1973a,b; Brown &

*Octahedral distortion is defined by $\Delta = 1/6 \sum_{i=1}^{6} [(R_i - \bar{R})/\bar{R}]^2$, where $\bar{R}$ = mean bond length and R_i = individual bond length.

Shannon 1973; Shannon 1974, 1976). That this is an important effect in orthopyroxenes is immediately apparent from the mean bond lengths and bond-length distortions in the *M*1 and *M*2 sites in $MgSiO_3$, $FeSiO_3$ and $ZnSiO_3$. In each case, the <*M*2-O> bond length is significantly larger than the <*M*1-O> bond length (by 0.076, 0.093 and 0.137Å respectively), despite the fact that both sites are occupied by the same cation; as these differences are considerably larger than the total variation in cation radius in these crystals, it is apparent that this factor must be taken into account when considering mean bond-length – cation-radius relationships. Brown & Shannon (1973) showed that mean bond length is, to a first approximation, a linear function of the bond-length distortion. Thus, in a series of isostructural compounds, the bond-length distortion must vary linearly with the cation radius if the mean bond length is to be a linear function of the cation radius. Inspection of Table 7 shows that this is not the case for either of the octahedral sites in the synthetic orthopyroxenes examined here. Comparison of Table 7 and Figure 4 shows that the amount of deviation of the data from a line through $MgSiO_3$ and $FeSiO_3$ correlates with the amount of distortion in excess of that forecast by interpolation between $MgSiO_3$ and $FeSiO_3$. This may be put on a more quantitative basis in the following manner. In a simple hard-sphere model, the mean bond length in a crystal should be equal to the sum of the cation and anion radii. If the *M*1 site in orthoenstatite is taken as the mean bond length for a Mg octahedron, the mean bond lengths for the orthopyroxenes in Table 7 may be forecast by adding the difference in constituent-cation radius to the <*M*1-O> distance in orthoenstatite, together with a small correction (0.007Å) for differences in anion coordination number when the *M*2 site is considered. The difference between these forecast values and the observed mean bond lengths should then represent the effect of bond-length distortion on the mean bond lengths. Table 8 lists these forecast values and the differ-

TABLE 6. MAGNITUDE AND ORIENTATION OF THE PRINCIPAL AXES OF THE THERMAL ELLIPSOIDS.

	R.M.S. Displacement (Å²)	Angle to a-axis(°)	Angle to b-axis(°)	Angle to c-axis(°)
		Orthoenstatite		
M1	0.059(3)	83(3)	92(4)	7(3)
	0.090(2)	108(25)	162(25)	90(5)
	0.094(2)	19(24)	108(25)	97(3)
M2	0.070(3)	71(3)	96(4)	20(2)
	0.099(2)	112(7)	157(8)	88(4)
	0.110(2)	150(6)	68(8)	70(2)
S1A	0.058(2)	88(4)	88(4)	3(5)
	0.077(2)	156(10)	114(10)	87(5)
	0.084(2)	114(10)	24(10)	91(3)
S1B	0.059(2)	86(4)	92(4)	5(5)
	0.077(2)	154(12)	64(12)	85(5)
	0.084(2)	64(12)	26(12)	90(4)
O1A	0.067(5)	93(19)	88(6)	3(16)
	0.078(4)	177(19)	91(9)	93(19)
	0.100(4)	91(9)	2(7)	92(6)
O2A	0.081(5)	54(15)	37(78)	82(229)
	0.082(5)	93(138)	78(188)	168(150)
	0.109(4)	144(6)	55(6)	81(7)
O3A	0.061(6)	86(7)	73(5)	17(5)
	0.094(4)	166(14)	76(14)	90(8)
	0.106(4)	76(14)	22(10)	107(5)
O1B	0.073(5)	92(21)	94(11)	4(16)
	0.082(4)	163(14)	107(14)	93(22)
	0.096(4)	107(14)	18(14)	87(10)
O2B	0.072(5)	76(10)	102(12)	19(15)
	0.086(4)	55(10)	139(10)	109(15)
	0.105(4)	39(9)	51(9)	95(7)
O3B	0.058(6)	97(6)	71(5)	21(5)
	0.093(4)	159(20)	111(20)	90(10)
	0.101(4)	109(21)	29(16)	111(5)
		Mg,Mn,Co Orthopyroxene		
M1	0.067(4)	69(15)	95(46)	22(9)
	0.070(4)	105(21)	165(20)	89(44)
	0.082(3)	154(10)	76(13)	58(9)
M2	0.069(3)	66(3)	91(4)	22(3)
	0.094(2)	118(8)	150(8)	79(5)
	0.109(2)	143(7)	60(8)	70(3)
S1A	0.070(3)	103(14)	85(23)	14(9)
	0.075(3)	118(14)	152(14)	91(25)
	0.084(2)	149(12)	63(13)	104(9)
S1B	0.066(3)	63(7)	90(15)	27(7)
	0.076(3)	76(14)	165(14)	97(15)
	0.084(3)	150(9)	105(14)	64(7)
O1A	0.070(7)	9(22)	92(9)	99(22)
	0.084(7)	99(22)	95(16)	169(21)
	0.103(6)	89(9)	5(15)	95(16)
O2A	0.078(7)	111(14)	144(20)	62(31)
	0.087(7)	110(16)	111(28)	150(31)
	0.113(5)	150(9)	62(8)	81(10)
O3A	0.070(8)	91(13)	60(6)	30(6)
	0.095(6)	177(13)	89(14)	92(12)
	0.115(5)	88(13)	30(6)	120(6)
O1B	0.072(8)	117(16)	126(12)	47(17)
	0.089(6)	133(29)	105(27)	133(22)
	0.097(6)	125(27)	40(16)	74(25)
O2B	0.070(8)	73(9)	123(13)	38(16)
	0.089(7)	65(12)	131(14)	128(16)
	0.113(5)	31(9)	59(9)	87(9)
O3B	0.068(8)	91(21)	62(7)	28(7)
	0.084(6)	174(10)	96(13)	88(19)
	0.113(5)	96(9)	28(7)	118(6)

ential values and the differ-

TABLE 7. MEAN BOND LENGTHS (Å), CONSTITUENT CATION RADII (Å) AND BOND LENGTH DISTORTIONS IN SYNTHETIC ORTHOPYROXENES

	<M1-O>	r_{M1}	Δ^*_{M1}	<M2-O>	r_{M2}	Δ^*_{M2}	Reference
$MgSiO_3$	2.076	0.720	0.85	2.149	0.720	5.75	This study
$MgSiO_3$	2.076	0.720	0.83	2.151	0.720	5.74	Ghose & Wan (1976)
$FeSiO_3$	2.135	0.780	0.43	2.228	0.780	10.18	Sueno et al. (1976)
$ZnSiO_3$	2.128	0.740	2.99	2.265	0.740	31.67	Morimoto et al. (1975)
$(Mg,Cu)SiO_3$	2.078	0.720	0.90	2.160	0.722	7.99	Ghose & Wan (1976)
$ZnMgSi_2O_6$	2.091	0.727	1.03	2.195	0.733	13.89	Morimoto et al. (1975)

*$\Delta = \Delta \times 10^3$.

TABLE 8. CALCULATED <M-O> (Å) DISTANCES IN SYNTHETIC ORTHOPYROXENES

	<M1-O>$_{calc}$	δ<M1-O>	Δ'^*	<M2-O>$_{calc}$	δ<M2-O>	Δ'^*
$MgSiO_3$	(2.076)	(0.000)	(0.00)	2.069	0.080	4.90
$FeSiO_3$	2.136	-0.001	-0.42	2.129	0.010	9.33
$ZnSiO_3$	2.096	0.032	2.14	2.089	0.176	30.82
$ZnMgSi_2O_6$	2.083	0.008	0.18	2.082	0.113	13.04
$(Mg,Cu)SiO_3$	2.076	0.002	0.05	2.071	0.089	7.14

* Δ' = difference in bond length distortion between the site and the M1 site in orthoenstatite; $\Delta' = \Delta'^* \times 10^3$.

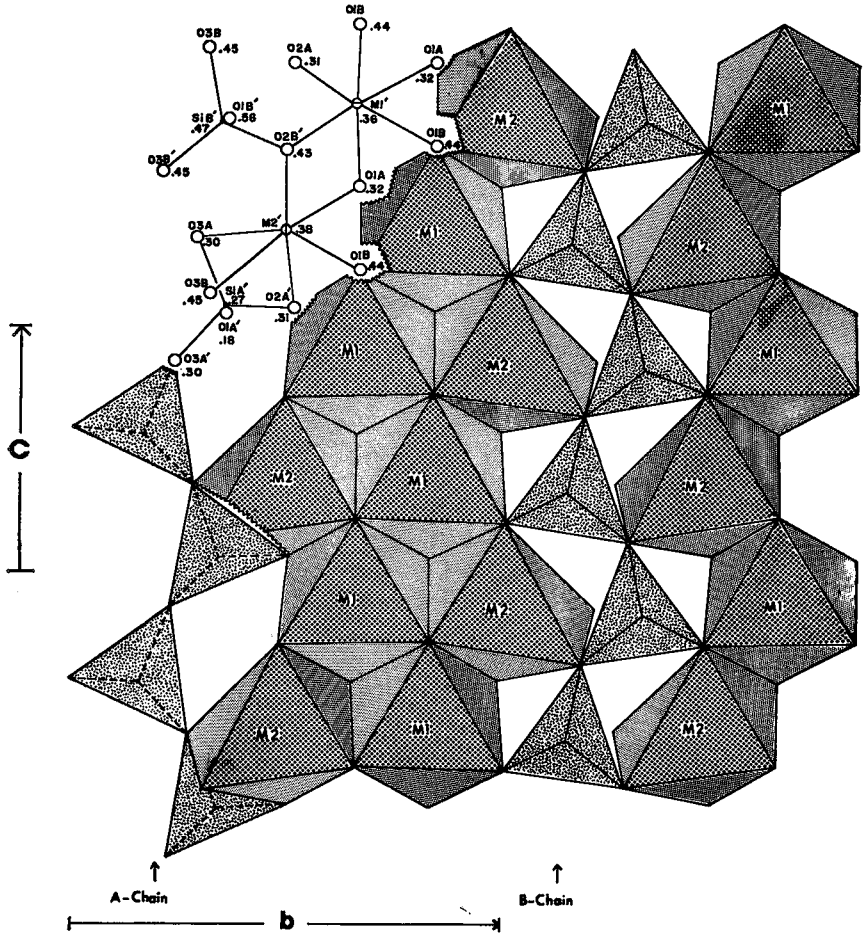

FIG. 3. The orthopyroxene structure projected down the *a* axis.

ence in distortion between the octahedra and the *M*1 octahedron in orthoenstatite. Figure 5 shows the relationship between the difference of the observed and calculated mean bond lengths and the bond-length distortion. Despite the fact that several different cations are involved, an extremely strong non-linear correlation is exhibited, suggesting that the amount of bond-length variation not attributable to cation-radius variations occurs as a result of bond-length distortion. One notable feature of Figure 5 is that there appears to be two separate trends for the *M*1 and *M*2 sites. This occurs as a result of the difference in the amount of distortion at each site, the *M*1 distortions being far smaller than the *M*2 distortions. Brown & Shannon (1973) developed linear relationships between mean bond length and distortion by second-order binomial expansion of their bond-strength equation; as they indicated, this approximation was valid for small distortions, but where the distortions are large, higher-order terms cannot be neglected. This is the origin of the non-linearity in Figure 4. For example, their distortional equation for Zn together with the distortions for $ZnSiO_3$ given in Table 7 forecast a $<M1\text{-}O>$ distance of 2.128Å, in agreement with the experimental results; high-order terms have negligible effect. However, for the *M*2 site their equation forecasts a $<M2\text{-}O>$ of 2.311Å, greatly in excess of the actual value of 2.265Å; using higher-order terms, a value of 2.281Å is forecast, with terms up to the eighth order contributing significantly (the 0.02Å difference between the observed and calculated values is not significant here as a 10% change in the bond-strength exponent gives perfect agreement, and this is within the limits of confidence of the exponent – Brown & Wu 1976). Thus, in the synthetic orthopyroxenes, the relationships between the mean

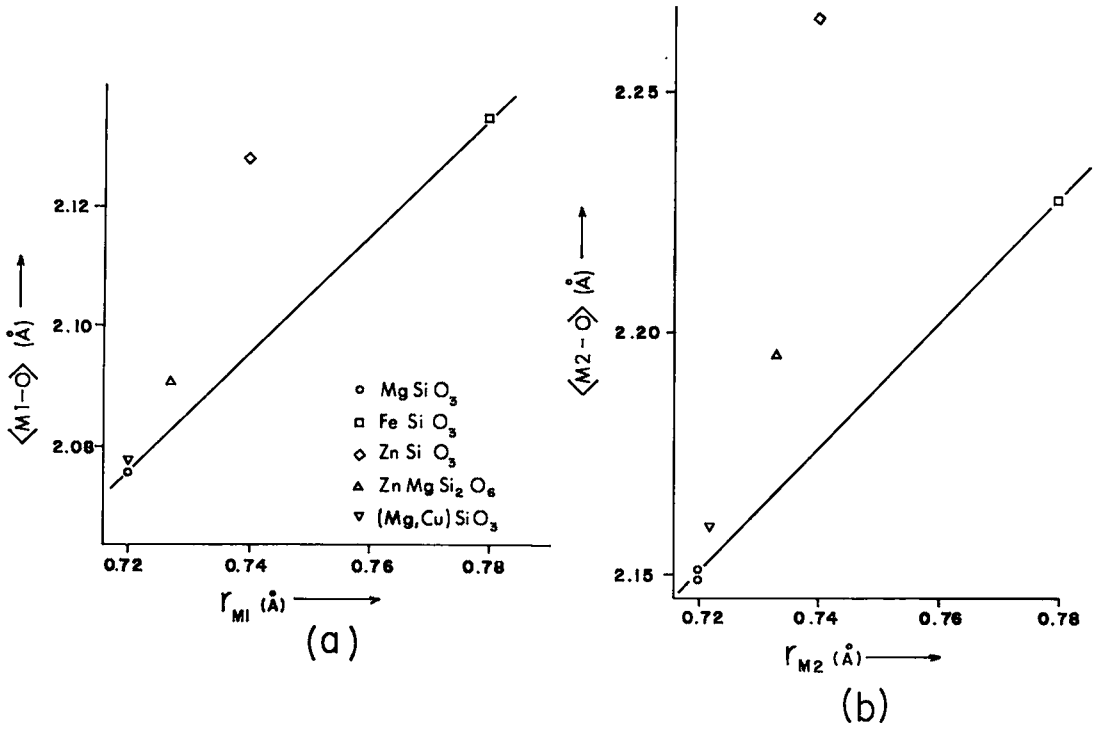

FIG. 4. Variation of <*M*-O> bond length with constituent-cation radius for synthetic orthopyroxenes.

bond length and constituent-cation radii for the *M*1 and *M*2 sites are non-linear as a result of the non-linear variation of bond-length distortion with constituent-cation radii.

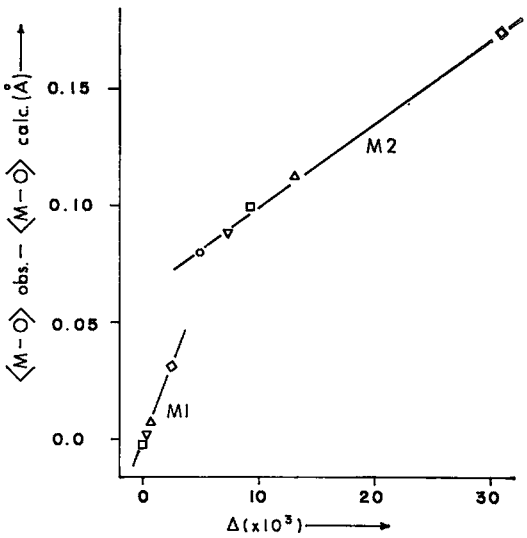

FIG. 5. Variation in the difference between the observed and calculated <*M*-O> bond lengths with the difference in octahedral bond-length distortion between the octahedron and the *M*1 octahedron in orthoenstatite. Legend as for Figure 4.

Turning to the natural orthopyroxenes, Table 9 lists the mean bond lengths, constituent-cation radii and bond-length distortion parameters for the refined orthopyroxenes. Previous workers have examined mean bond-length variations as a function of Mg/Fe^{2+} site-occupancy. Most natural orthopyroxenes contain significant amounts of Ca, Ti, Cr, Mn, Fe^{3+} and Al; because of the disparate size of these cations, the presence of even small amounts in a site will significantly affect the mean bond length of that site. In the present study, <*M*-O> bond-length variation is examined as a function of the mean ionic radius of the constituent cations in a site; Ti, Cr, Fe^{3+} and Al^{VI} were assumed to occupy *M*1 with Ca and Mn in *M*2. Figure 6 shows the variation in mean octahedral bond lengths as a function of the mean constituent-cation radius, where the radii have been calculated both with and without the contributions of the minor cations (Table 9).

Because the bulk chemical composition of natural orthopyroxenes is much more complex than synthetic orthopyroxenes, additional factors that may affect mean bond-length – ionic-radius relationships require consideration. Recent

studies of natural orthopyroxenes by transmission electron microscopy (Champness & Lorimer 1974; Kohlstedt & Vander Sande 1973; Vander Sande & Kohlstedt 1974) have revealed the presence of complex microstructures. The type of microstructure appears to be a function of the Ca content of the bulk crystal (Boland 1972; Champness & Lorimer 1973) and there is some evidence of compositional differences between host orthopyroxene and microstructure (Lorimer & Champness 1973). Three distinct precipitate phases were identified by Champness & Lorimer (1974) in Stillwater and Bushveld orthopyroxenes: coarse augite lamellae, fine $P2_1/c$ lamellae of pigeonitic composition, and Guinier-Preston (G.P.) zones that show evidence of enrichment in calcium. Clinoenstatite lamellae have also been identified (Boland *et al.* 1973; Iijima & Buseck 1975) and it has been suggested (Boland 1974) that augite lamellae form from the clinoenstatite lamellae by taking up Ca from the host orthopyroxene during cooling.

These findings indicate that the minor components in orthopyroxene may preferentially occur in microstructures rather than in the host orthopyroxene. This being the case, two situations may be recognized: the microstructures may be small enough to diffract X-rays coherently with respect to the diffraction from the host lattice, and thus will contribute to the diffraction pattern of the orthopyroxene. Alternatively, microstructures may be large enough to diffract X-rays incoherently with respect to the diffraction from the host lattice, and thus will not contribute to the diffraction pattern of the orthopyroxene host due to the mis-registry of the two reciprocal lattices. Thus, the minor components present in the bulk sample analysis may occur in the host orthopyroxene and/or in small microstructures, where they will contribute to the diffraction pattern, and in larger microstructures where they will not contribute to the orthopyroxene diffraction pattern.

Figure 7 shows the variation in bond-length distortion with constituent-cation radius for the octahedra in natural orthopyroxenes. For the *M*1 site, the bond-length distortion decreases with increasing size; deviations from linearity of up to $\sim 0.2\Delta(\times 10^{-3})$ occur. These will produce bond-length changes of ~0.001Å and consequently this factor is negligible for the *M*1 octahedron. Examination of Figures 6a and 6c show that when the effects of minor components are included in the cation radius, a linear relationship results. However, there is some scatter in the data, with deviations of up to ±0.007Å. In addition, the slope of the curve is ~0.87, significantly less than that expected for a relationship

TABLE 9. MEAN BOND LENGTHS (Å), CONSTITUENT CATION RADII (Å) AND BOND LENGTH DISTORTIONS IN NATURAL ORTHOPYROXENES.

	⟨M1-O⟩	r^{*}_{M1}	r^{**}_{M1}	Δ^{+}_{M1}	M2-O	r^{*}_{M2}	r^{**}_{M2}	Δ^{+}_{M2}	Ref.
Ferrohypersthene	2.104	0.745	0.745	0.50	2.222	0.783	0.776	8.68	1
Eulite	2.123	0.760	0.765	0.41	2.224	0.788	0.779	9.18	2
Bronzite	2.079	0.721	0.722	0.62	2.172	0.746	0.739	5.88	3
Bronzite	2.080	0.719	0.723	0.69	2.185	0.762	0.748	5.66	4
Bronzite	2.080	0.720	0.721	0.78	2.171	0.740	0.738	5.89	4
Bronzite	2.083	0.719	0.726	0.67	2.200	0.770	0.746	5.65	5
Bronzite	2.087	0.723	0.728	0.69	2.197	0.765	0.744	6.32	6
Al bronzite	2.070	0.708	0.721	0.80	2.176	0.757	0.739	4.64	7
Hypersthene	2.085	0.716	0.724	0.64	2.201	0.783	0.771	6.47	8
Al bronzite	2.053	0.680	0.724	0.81	2.156	0.744	0.742	3.05	8
Al bronzite	2.053	0.683	0.727	0.89	2.156	0.741	0.739	3.33	8

References: 1 – Smyth 1973; 2 – Burnham et al. 1971; 3 – Dodd et al. 1975; 4 – Miyamoto et al. 1975; 5 – Takeda & Ridley 1972; 6 – Ghose & Wan 1973; 7 – Takeda 1972; 8 – Kosoi et al. 1974.

*includes minor components, **excludes minor components, $\Delta = \Delta_x \times 10^3$

TABLE 10. MEAN BOND LENGTHS (Å) AND Al CONTENTS OF TETRAHEDRA IN NATURAL ORTHOPYROXENES

Al^{IV}	⟨SiA-O⟩	⟨SiB-O⟩	⟨t⟩*	⟨t'⟩**	Reference
0.000	1.628	1.640	0.260	0.260	This study
0.000	1.626	1.637	0.260	0.260	Suena et al. (1976)
0.150	1.627	1.645	0.280	0.270	Takeda (1972b)
0.054	1.629	1.641	0.267	0.260	Ghose & Wan (1973)
0.059	1.625	1.639	0.268	0.260	Takeda & Ridley (1973)
0.058	1.627	1.640	0.268	0.260	Kosoi et al. (1974)
0.248	1.627	1.663	0.292	0.283	Kosoi et al. (1974)
0.248	1.628	1.656	0.292	0.280	Kosoi et al. (1974)
0.021	1.625	1.639	0.263	0.260	Burnham et al. (1971)
0.052	1.626	1.637	0.267	0.260	Dodd et al. (1975)
0.042	1.625	1.641	0.265	0.260	Miyamoto et al. (1975)

*calculated assuming all Al^{IV} is in SiB** calculated assuming some Al^{IV} in incoherently diffracting microstructures.

TABLE 11. ⟨M2-O⟩ DISTANCES (Å), CORRECTED FOR NON-LINEAR BOND LENGTH DISTORTION.

All Ca in M2			No Ca in M2			Reference
r_{M2}(Å)	Δ''*	⟨M2-O⟩corr.	r_{M2}(Å)	Δ''*	⟨M2-O⟩corr.	
0.783	1.72	2.233	0.776	1.21	2.230	Smyth (1973)
0.788	1.42	2.233	0.779	0.92	2.230	Burnham et al. (1971)
0.746	1.76	2.183	0.739	1.25	2.180	Dodd et al. (1975)
0.762	3.17	2.205	0.748	2.14	2.199	Miyamoto et al. (1975)
0.740	1.32	2.179	0.738	1.18	2.178	Miyamoto et al. (1975)
0.770	3.78	2.224	0.746	1.98	2.213	Takeda & Ridley (1972)
0.765	3.48	2.219	0.744	1.15	2.204	Ghose & Wan (1973)
0.757	3.83	2.200	0.739	2.49	2.192	Takeda (1972)
0.783	3.93	2.226	0.771	3.03	2.220	Kosoi et al. (1974)
0.744	4.45	2.184	0.742	4.31	2.183	Kosoi et al. (1974)
0.741	3.95	2.180	0.739	3.80	2.179	Kosoi et al. (1974)

* Δ'' = deviation from linearity in Figure 7b.

of this sort where distortion does not materially contribute to mean bond-length variations along the series. When the minor components are not included in the cation-radius estimation, 80% of the data becomes colinear with orthoenstatite and orthoferrosilite, suggesting that the octahedral trivalent cations reside in incoherently-diffracting microstructures. The slope of the linear relationship is ~0.98, close to the ideal value of 1.0. The data that deviate from this relationship (Takasima bronzite, Takeda 1972b; #2 and 3, Kosoi *et al.* 1974) are characterized by much higher trivalent-cation occupancies of both octahedral and tetrahedral sites. If the octahedral trivalent cations are assumed to occur in both the host crystal (and coherently-diffracting microstructures) and incoherently-diffracting microstructures, then these crystals also can be

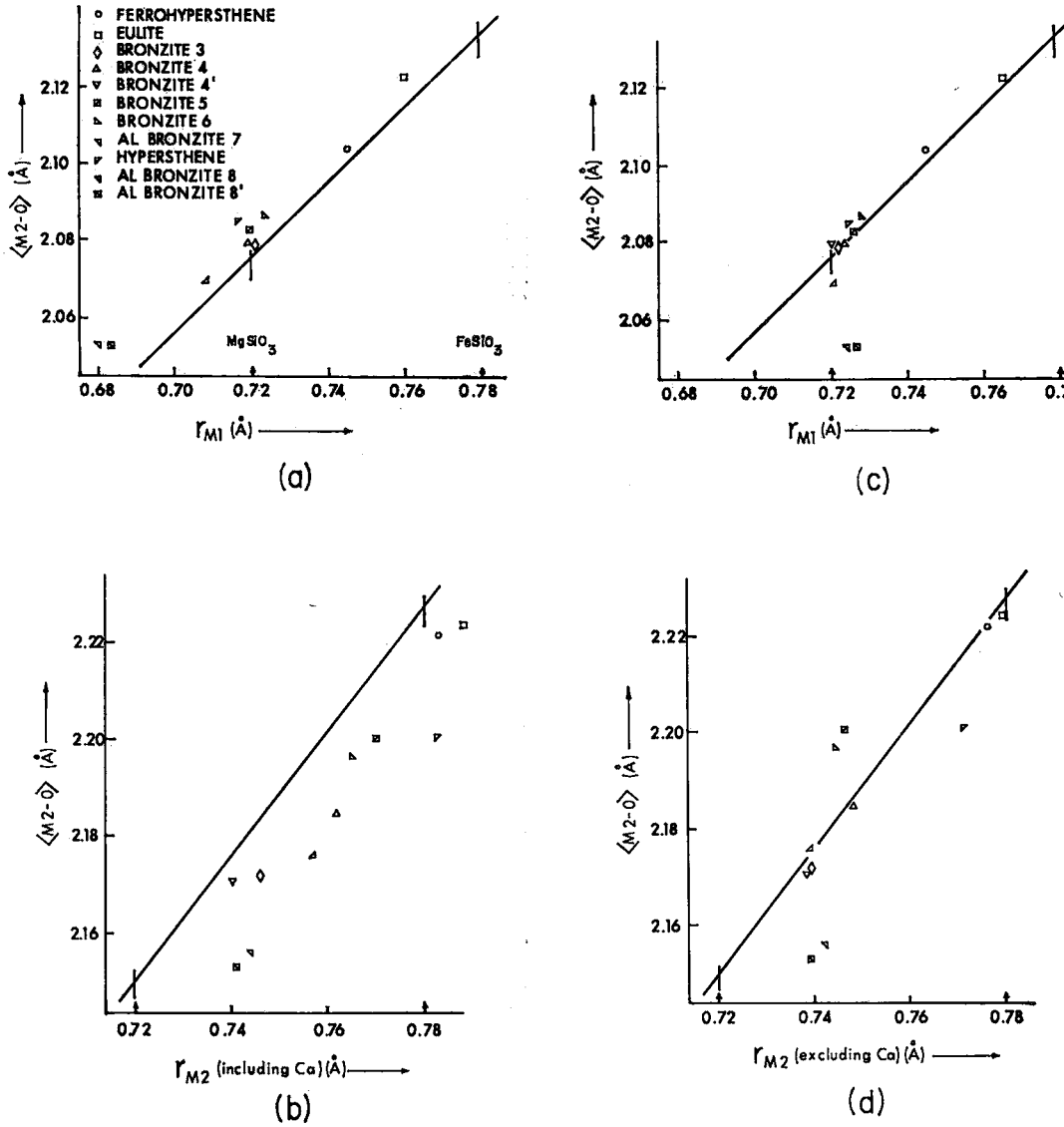

FIG. 6. Variation of <*M*-O> bond length with constituent-cation radius for natural orthopyroxenes. (a) & (b): relationships for the *M*1 and *M*2 octahedra where the minor components have been included in the cation-radius calculation. (c) & (d): relationships for the *M*1 and *M*2 octahedra where the minor components have been excluded from the cation-radius calculation.

colinear with the rest of the data. Additional evidence concerning the concentration of trivalent cations in incoherent microstructures is gained from an examination of the mean bond-length – cation-radius relationships for the tetrahedra. Takeda (1971, 1972a) showed that tetrahedral Al preferentially occupies the Si*B* tetrahedron in orthopyroxene, and this has since been confirmed by Kosoi *et al.* (1974). Table 10 summarizes the available data. The <Si*A*-O> distance is virtually constant at 1.627Å, confirming that any tetrahedral Al occupies the Si*B* tetrahedron. Figure 8a shows the variation in <Si*B*-O> as a function of tetrahedral Al; as distortional effects are negligible in this case and comparison of the bond lengths in orthoenstatite and orthoferrosilite indicate that bond lengths change only very slightly with the Mg/Fe ratio, this relationship should be defined by a straight line with slope of 1.0 and an intercept of ~1.639Å.

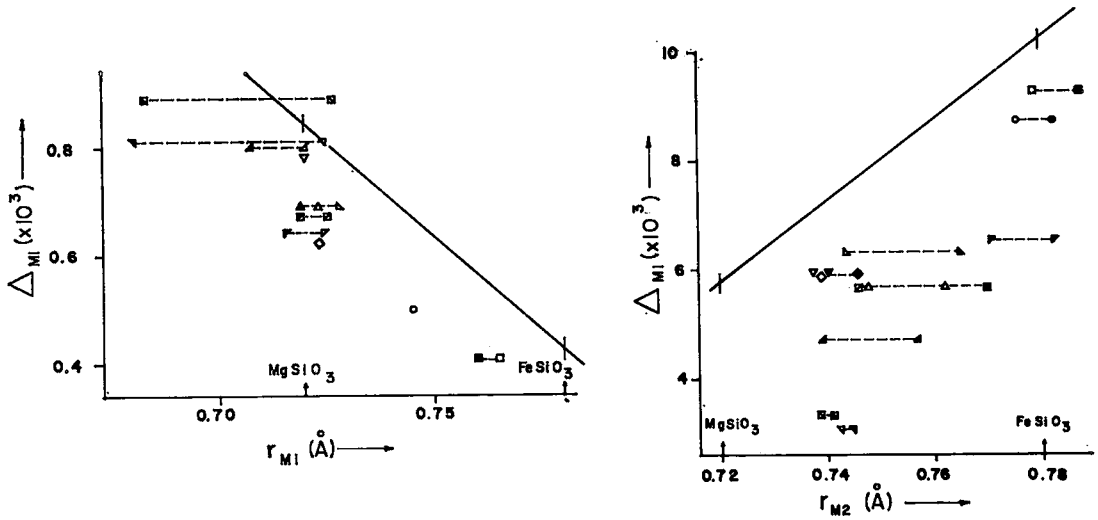

FIG. 7. Variation of octahedral bond-length distortion with constituent-cation radius for the *M*1 and *M*2 octahedra in natural orthopyroxenes. Legend as for Figure 6; solid symbols correspond to data where the minor components were included in the cation-radius calculation; empty symbols correspond to data where the minor components were excluded from the cation-radius calculation.

Deviations of up to 0.015Å from this ideal relationship occur; the data have a rather ill-defined relationship with a slope of ~0.7. Trivalent cations will be incorporated into the orthopyroxene lattice by a substitution of the form $2M^{3+} \rightleftharpoons (Mg,Fe^{2+})+Si$; thus trivalent cations, particularly Al (Anastasion & Seifert 1972), may be incorporated into the orthopyroxene lattice in considerable amounts. However, it was shown earlier that octahedral trivalent cations may preferentially occur in incoherently-diffracting microstructures. This being the case, a corresponding amount of tetrahedral trivalent cations would also be incorporated into these microstructures and would not contribute to tetrahedral bond-length variations in the host crystal. For all orthopyroxenes with Al^{VI} <0.06, the <Si*B*-O> is 1.639Å, suggesting that Al does not contribute to this site; these are the same orthopyroxenes which were colinear with orthoenstatite and orthoferrosilite when the octahedral trivalent cations were not considered in the cation radius. For the remaining orthopyroxenes (Takasima bronzite, Takeda 1972b; #2 and 3, Kosio *et al.* 1974), the Al^{IV} will be partitioned between orthopyroxene and incoherently-diffracting microstructures in the same ratio as the octahedral trivalent cations; this ratio was calculated for each of these samples by assuming that they are colinear with orthoenstatite and orthoferrosilite on a <*M*1-O>-r_{M1} plot. Figure 8b shows the resulting <Si*B*-O>-r_{SiB} relationship following this procedure; the maximum deviation from the ideal relationship is reduced from 0.015Å to 0.004Å, and the relationship is now more linear. This improvement for the Si*B* site supports our argument that the octahedral trivalent cations may or may not contribute to *M*1 bond-length variations, depending on whether they occur in the host crystal and coherently-diffracting microstructures, or in incoherently-diffracting microstructures.

Figure 7b shows the variation in bond-length distortion with constituent-cation radius for the *M*2 octahedron in natural orthopyroxenes; as with the synthetic orthopyroxenes, the variation in distortion is non-linear. As all the departures from linearity are negative in Δ, the observed mean bond lengths will be less than those forecast from the *M*2 cation radius by interpolation between orthoenstatite and orthoferrosilite. In agreement with this, all natural orthopyroxenes fall below the orthoenstatite-orthoferrosilite line in Figure 6b. However, an additional complication is introduced by the presence of Ca, which may be preferentially concentrated in incoherently-diffracting microstructures. Figure 6d shows the variation in <*M*2-O> with *M*2 cation radius, where the contribution of Ca to the cation radius was not considered. Although much of the data are now colinear with orthoenstatite and orthoferrosilite, as indicated by Morimoto (1974), the lunar pyroxenes (Takeda & Ridley 1972; Ghose & Wan 1973) and the three pyroxenes refined by Kosoi *et al.* (1974) show deviations from linearity of +0.017Å and −0.021Å,

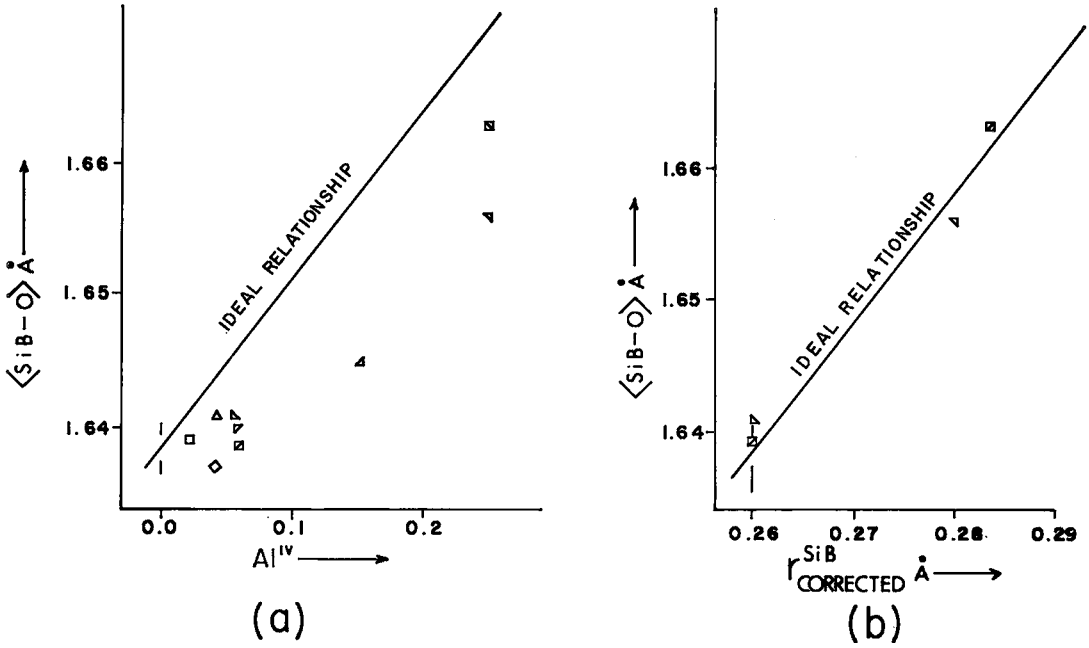

FIG. 8. Variation of <Si*B*-O> bond length with constituent-cation radius. (a) : cation radius calculated assuming all tetrahedral Al in Si*B* tetrahedron. (b): cation-radius values taken from Table 10. Legend as for Figure 6.

respectively. The positive deviations exhibited by the lunar pyroxenes could be explained by approximately equal partition of Ca between the host orthopyroxene (and coherently-diffracting microstructures) and incoherently-diffracting microstructures. However, the negative departures from linearity cannot be accounted for by this reasoning; it is notable that the three orthopyroxenes showing negative deviations from linearity also show the largest departures from a linear bond-length distortion – *M*2 cation-radius relationship (Figure 7b). The amount of departure of the data from the orthoenstatite-orthoferrosilite line in Figure 7b may be used to estimate corrections for <*M*2-O>, arising from the non-linear variation in distortion. This has been done both with and without the contribution of Ca; the corrections are listed in Table 11. It should be noted that these are only first-order corrections as higher-order correction terms cannot be calculated. However, calculation of higher-order terms for orthoenstatite and orthoferrosilite indicate that these will affect the mean bond lengths by 0.01Å at the most. Figure 9 shows the variation in <*M*2-O> (corrected for non-linear variation in distortion) with *M*2 cation radius (calculated both with or without the contribution of Ca). When Ca is considered as completely contributing to the *M*2 cation radius, the relationship is fairly linear, with the maximum deviation of 0.01Å exhibited by the lunar pyroxenes (Takeda & Ridley 1972; Ghose & Wan 1973). When the Ca contribution is not considered, deviations from linearity are much larger. However, as indicated above, second-order corrections may reduce <*M*2-O> (corrected) by up to 0.01Å, reducing the positive deviations of the 'no Ca' data points and producing negative deviations for the 'all Ca' data points, and indicating a partial contribution of Ca to the *M*2 cation radius. However, structure refinements are needed on synthetic orthopyroxenes along the orthoenstatite-orthoferrosilite join in order to characterize these higher-order corrections before this question is resolved.

In the above discussion, it was assumed that the microstructures either diffracted coherently or incoherently with respect to the host crystal, and that in the latter case, the reciprocal lattices did not overlap. At lower angles, there may be some overlap, resulting in an incoherent contribution from the microstructures; in addition, partial coherence may occur. The effects of these processes are difficult to evaluate, although there is some evidence (Berking & Jagodzinski 1973) that this may significantly affect the atomic positions derived from the refinement.

Site-occupancies in (Mg,Mn,Co) orthopyroxene

The results of the site-occupancy refinement for the (Mg,Mn,Co) orthopyroxene are as follows: $M1$=0.904(4)Mg+0.096Fe*, $M2$=0.65Mg +0.342Fe*. It is apparent from these results that the transition metals are strongly ordered into the $M2$ site, in agreement with the predictions of Burns (1970a).

The individual Mn and Co site-occupancies are of interest and the site-population refinement does not provide sufficient information to derive these. However, unique site-populations may be derived from the mean bond lengths in the following manner. The bond-length distortion for the $M1$ site is 0.81 ($\times 10^{-3}$); as the cation radius of $M1$ will only be slightly larger than that of Mg, this distortion is colinear with orthoenstatite & orthoferrosilite (Figure 5a). Thus the data point for this sample should be colinear with orthoenstatite and orthoferrosilite. $<M1\text{-O}>$ is 2.079Å, which corresponds to a cation radius of 0.723Å; using the ionic radii (Mg=0.720, Mn=0.830, Co^{2+}=0.745Å; R. D. Shannon, pers. comm. 1975), in conjunction with the refined Fe* site-occupancy for $M1$, give the following site-populations: $M1$= 0.904Mg+0.065Co^{2+}+0.031Mn^{2+}. The resultant $M2$ site-population is: $M2$=0.658Mg+ 0.198Co^{2+}+0.144Mn^{2+}. This is in accord with the site-preference of Co in (Mg,Co) orthopyroxene and Mn in (Mg,Mn) low ($P2_1/c$) clinopyroxene (Ghose *et al.* 1974, 1975).

The configuration of the silicate chains

As indicated by previous workers (Burnham 1967; Morimoto & Tokonami 1969), there are two crystallographically distinct silicate chains in the orthopyroxene structure. In a detailed discussion of pyroxene topology, Papike *et al.* (1973) showed how the structure is put together in violation of Thompson's (1970) parity rule by rotation and extension of the A-chains to form O-rotated configurations in all layers. As a consequence of this, the tetrahedra of the A-chains share an edge with the very distorted $M2$ octahedra, but the tertahedra of the B-chains do not (Fig. 3). This leads to a considerable difference in the distortion of the silicate tetrahedra in the two chains (see Table 5). The shared edge in the A-chain tetrahedra is contracted (O2A-O3A' ~2.49Å, O2A-SiA-O3A' ~100°) relative to both the other edges of the same tetrahedron and the corresponding edges (unshared) in the B-chain tetrahedra (O2B-O3B ~2.59 & 2.67Å, O2B-SiB-O3B ~105 & 110°) due to cation-cation repulsion between SiA and $M2$. However, this is not the only factor affecting the

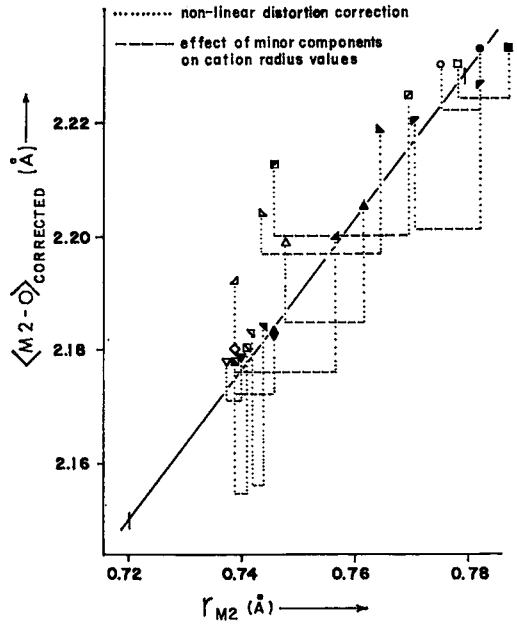

FIG. 9. Variation of $<M2\text{-O}>$ bond length, corrected for non-linear distortion effects, with constituent-cation radius. Legend as for Figure 6; solid symbols correspond to data where minor components were included in the cation-radius calculation; empty symbols correspond to data where the minor components were excluded from the cation-radius calculation.

relative distortion of the different chains. As mentioned previously, the A-chain is considerably more extended than the B-chain in order to reduce the parity violation in this structure. As both chains are formed by c-glide repeat of a single tetrahedron, the overall repeat distance is the same in both cases. Because the A-chain is straighter than the B-chain, the SiB tetrahedron must be elongated in the c direction relative to the SiA tetrahedron. Inspection of Table 5 shows that this is so; $<$SiA-O3$A>$ ~1.655Å and $<$SiB-O3$B>$ ~1.674Å. Similarly O3B-O3B' (~2.76Å) is considerably larger than O3A-O3A' (~2.63Å), with a corresponding increase in the bond angle at the central cation (O3A-SiA-O3A' ~105.5°, O3B-SiB-O3B' ~111.1°). Another feature of note is the constancy of the Si-O2 bond length and O1-Si-O2 bond angle, both between the two chains, and in both orthopyroxenes refined in the present study. In general in the orthopyroxenes, SiA-O2A and SiB-O2B $\leq$1.60Å, a feature that is also shown by the clinopyroxenes (Clark *et al.* 1968) and the non-Al^{IV} amphiboles. This is a result of the bond-strength requirements of the O2(A,B) (pyroxene)

and O(4) (amphibole) anions, both of which are formally underbonded in a Pauling (1960) bond-strength scheme (Ghose 1961, 1965; Baur 1970, 1971; Hawthorne 1973). Thus the principal causes of the relative distortion of Si*B* are relaxation due to cation-cation repulsion and *c*-axis elongation, operating under the constraint that the Si*B*-O2*B* bond must remain short. This leads to much larger bond-length distortion in the *B*-chain tetrahedra which, in some measure, accounts for the fact that <Si*B*-O> is significantly larger than <Si*A*-O>.

Examination of the empirical bond-strength table for orthoenstatite (Table 12), calculated from the curves of Brown & Shannon (1973), indicates that the extreme bond-length distortions observed in this structure are a result of the anion bond-strength requirements. Although the anion bond-strength sums deviate somewhat from ideality, it is apparent that the dominant factors in the bond-length distortions are a strengthening of the bonds to the O2*A* and O2*B* anions and a weakening of the bonds to the O3*A* and O3*B* anions. Superimposed on these are the effects of structural relaxation due to cation-cation repulsion. It was shown above that this has a strong influence on the relative distortion of the *B*-chain Si tetrahedra. Examination of Table 5 shows that it is also present in the octahedral part of the structure. The *M*1 octahedron shares five edges with adjacent octahedra, two with neighboring *M*1 octahedra, and three with *M*2 octahedra. In all cases, the lengths of the shared edges (<2.85Å) are less than those of the unshared edges (>2.85Å) for both structures refined in this study. This is also reflected in the bond angles subtended by these edges, all of which are ≤87.8°; however, the division between shared and unshared elements is not as complete for the bond angles. Although all angles subtending shared edges are less than the angles subtending unshared elements in the *M*1 octahedron, this is not so for the *M*2 octahedron (Table 5).

TABLE 12. EMPIRICAL BOND STRENGTH TABLE FOR ORTHOENSTATITE

	M1	M2	SiA	SiB	Σ
O1A	0.384 0.300	0.339	1.027		2.050
O2A	0.402	0.381	1.095		1.878
O3A		0.229	0.887 0.944		2.060
O1B	0.288 0.354	0.364		1.008	2.014
O2B	0.371	0.415		1.092	1.878
O3B		0.172		0.867 0.871	1.910

In particular, the O3*A*-*M*2-O3*B* angles of 75.4 and 74.3° are considerably smaller than any of the O-*M*2-O angles subtending shared octahedral edges; however, the O3*A*-O3*B* edge is not extremely short, and this small angle is a result of the extremely long *M*2-O3*A*-O3*B* bonds.

Acknowledgments

We would like to thank the Materials Research Institute, McMaster University, Hamilton, for their cooperation in the collection of the intensity data, and Dr. Ian Steele, University of Chicago, for the microprobe analyses. Financial support was provided by the National Research Council of Canada (grant to R. B. Ferguson) and the University of Manitoba.

References

Anastasiou, P. & Seifert, F. (1972): Solid solubility of Al_2O_3 in enstatite at high temperatures and 1-5 kb water pressure. *Contr. Mineral. Petrology.* **34**, 272-287.

Bancroft, G. M., Burns, R. G. & Howie, R. A. (1967): Determination of the cation distribution in the orthopyroxene series by the Mössbauer effect. *Nature* **213**, 1221-1223.

Baur, W. H. (1970): Bond length variation and distorted coordination polyhedra in inorganic crystals. *Trans. Amer. Cryst. Assoc.* **6**, 129-155.

——— (1971): The prediction of bond length variations in silicon-oxygen bonds. *Amer. Mineral.* **56**, 1573-1599.

Berking, B. & Jagodzinski, H. (1973): Die Verfeinerung der Kristallstruktur eines lunaren Pigeonits. *Z. Krist.* **137**, 352-359.

Blander, M. (1970): The partitioning of cations between coexisting one site–two site phases. *Geochim. Cosmochim. Acta* **34**, 515-518.

——— (1972): Thermodynamic properties of orthopyroxenes and clinopyroxenes based on the ideal two-site model. *Geochim. Cosmochim. Acta* **36**, 787-799.

Boland, J. N. (1972): Electron petrography of exsolution in an enstatite-rich orthopyroxene. *Contr. Mineral. Petrology* **37**, 229-234.

——— (1974): Lamellar structures in low-calcium orthopyroxenes. *Contr. Mineral. Petrology* **47**, 215-222.

Brown, I. D. & Shannon, R. D. (1973): Empirical bond strength–bond length curves for oxides. *Acta Cryst.* **A29**, 266-282.

——— & Wu, K. K. (1976): Empirical parameters for calculating cation-oxygen bond valences. *Acta Cryst.* **B32** (in press).

Burnham, C. W. (1967): Ferrosilite. *Carnegie Inst. Wash. Yearbook* **65**, 285-290.

———, OHASHI, Y., HAFNER, S. S. & VIRGO, D. (1971): Cation distribution and atomic thermal vibrations in an iron-rich orthopyroxene. *Amer. Mineral.* **56**, 850-876.

BURNS, R. G. (1970a): *Mineralogical Applications of Crystal Field Theory*. Cambridge University Press, Cambridge, England.

——— (1970b): Site preferences of transition metal ions in silicate crystal structures. *Chem. Geol.* **5**, 275-283.

CHAMPNESS, P. E. & LORIMER, G. W. (1973): Precipitation (exsolution) in an orthopyroxene. *J. Mat. Sci.* **8**, 467-474.

——— & ——— (1974): A direct lattice-resolution study of precipitation (exsolution) in orthopyroxene. *Phil. Mag.* **30**, 357-365.

CLARK, J. R., APPLEMAN, D. E. & PAPIKE, J. J. (1968): Bonding in eight ordered clinopyroxenes isostructural with diopside. *Contr. Mineral. Petrology* **20**, 81-85.

CROMER, D. T. & MANN, J. B. (1968): X-ray scattering factors computed from numerical Hartree-Fock wave functions. *Acta. Cryst.* A**24**, 321-324.

——— & LIBERMAN, D. (1970): Relativistic calculation of anomalous scattering factors for X-rays. *J. Chem. Phys.* **53**, 1891-1898.

DODD, R. T., GROVER, J. E. & BROWN, G. E. (1975): Pyroxenes in the Shaw (L-7) chondrite. *Geochim. Cosmochim. Acta* **39**, 1585-1594.

DONNAY, G. & DONNAY, J. D. H. (1953): Crystal chemistry of some alkali silicates. *Amer. Mineral.* **38**, 163-171.

EVANS, B. J., GHOSE, S. & HAFNER, S. S. (1967): Hyperfine splitting of ^{57}Fe and Mg-Fe order-disorder in orthopyroxenes ($MgSiO_3$-$FeSiO_3$ solid solution). *J. Geol.* **75**, 306-322.

FINGER, L. W. (1969a): RFINE. A Fortran IV computer program for structure factor calculation and least-squares refinement of crystal structures. *Geophys. Lab. Carnegie Inst. Wash.* (unpubl.).

——— (1969b): Determination of cation distribution by least-squares refinement of single-crystal X-ray data. *Carnegie Inst. Wash. Yearbook* **67**, 216-217.

GHOSE, S. (1961): The crystal structure of cummingtonite. *Acta Cryst.* **14**, 622-627.

——— (1962): The nature of Mg^{2+}-Fe^{2+} distribution in some ferromagnesian minerals. *Amer. Mineral.* **47**, 388-394.

——— (1965a): Mg^{2+}-Fe^{2+} order in an orthopyroxene. *Z. Krist.* **122**, 81-99.

——— (1965b): A scheme of cation distribution in the amphiboles. *Mineral. Mag.* **35**, 46-54.

——— & HAFNER, S. S. (1967): Mg^{2+}-Fe^{2+} distribution in metamorphic and volcanic orthopyroxenes. *Z. Krist.* **125**, 157-162.

——— & WAN, C. (1973): Luna 20 pyroxenes: evidence for a complex thermal history. *Proc. Fourth Lunar Sci. Conf., Geochim. Cosmochim. Acta Suppl. 4, Vol.* **1**, 901-907.

——— & ——— (1976): Site preference of Cu^{2+}-ions in enstatite and the refinement of the crystal structure of pure enstatite. *Eos* **57**, 337 (Abstr.).

———, OKAMURA, F. P., WAN, C. & OHASHI, H. (1974): Site preference of transition metal ions in pyroxene and olivine. *Eos* **55**, 467 (Abstr.).

———, WAN, C. & OKAMURA, F. P. (1975): Site preference and crystal chemistry of transition metal ions in pyroxenes and olivines. *Acta. Cryst.* A**31**, Pt. S3, S76 (Abstr.).

GRANDIN, DE L'EPREVIER, A. (1972): *Synthèse de monocristaux de forsterite, Mg_2SiO_4 par la méthode des sels fondus.* Thèse, La Faculté Sci. d'Orléans, France.

GROVER, J. E. & ORVILLE, P. M. (1969): The partitioning of cations between coexisting single- and multi-site phases with application to the assemblages: orthopyroxene-clinopyroxene and orthopyroxene-olivine. *Geochim. Cosmochim. Acta* **33**, 205-226.

HAWTHORNE, F. C. (1973): *The Crystal Chemistry of the Clino-Amphiboles.* Ph.D. thesis, McMaster Univ., Hamilton, Ontario.

IIJIMA, S. & BUSECK, P. R. (1975): High resolution electron microscopy of enstatite. I: Twinning, polymorphism, and polytypism. *Amer. Mineral.* **60**, 758-770.

ITO, J. (1975): High temperature solvent growth of orthoenstatite, $MgSiO_3$, in air. *Geophys. Res. Lett.* **2**, 533-536.

KOHLSTEDT, D. L. & VANDER SANDE, J. B. (1973): Transmission electron microscopy investigation of the defect structure of four natural orthopyroxenes. *Contr. Mineral. Petrology* **42**, 169-180.

KOSOI, A. L., MALKOVA, L. A. & FRANK-KAMENETSKII, V. A. (1974): Crystal-chemical characteristics of rhombic pyroxenes. *Soviet Phys. Cryst.* **19**, 171-174.

KRETZ, R. (1961): Some applications of thermodynamics to coexisting minerals of varible composition. Examples orthopyroxene-clinopyroxene and orthopyroxene-garnet. *J. Geol.* **69**, 361-387.

——— (1963): Distribution of magnesium and iron between orthopyroxene and calcic pyroxene in natural mineral assemblages. *J. Geol.* **71**, 773-785.

LINDEMANN, W. (1961): Beitrag zur Enstatistruktur (Verfeinerung der Parameterwerte). *Neues Jahrb. Mineral. Monatsh.*, 226-233.

LORIMER, G. W. & CHAMPNESS, P. E. (1973): Combined electron microscopy and analysis of an orthopyroxene. *Amer. Mineral.* **58**, 243-238.

MATSUI, Y. & BANNO, S. (1970): Partition of divalent transition metals between coexisting ferromagnesian minerals. *Chem. Geol.* **5**, 259-265.

MAXEY, L. R. & VOGEL, T. A. (1974): Compositional dependence of the coexisting pyroxene

iron-magnesium distribution coefficient. *Contr. Mineral. Petrology* **43**, 295-306.

MEDARIS, L. G. (1969): Partitioning of Fe^{++} and Mg^{++} between coexisting synthetic olivine and orthopyroxene. *Amer. J. Sci.* **267**, 945-968.

MIYAMOTO, M. (1974): Crystallographic studies of a bronzite in the Johnston achondrite. *Int. Mineral. Assoc. Abstr.*, Berlin Meet., 153.

———, TAKEDA, H. & TAKANO, Y. (1975): Crystallographic studies of a bronzite in the Johnston achondrite. *Fortschr. Mineral.* **52**, 389-397.

MORIMOTO, N. (1974): Crystal structure and fine texture of pyroxenes. *Fortschr. Mineral.* **52**, 52-80.

——— & KOTO, K. (1969): The crystal structure of orthoenstatite. *Z. Krist.* **129**, 65-83.

———, NAKAJIMA, Y., SYONO, Y., AKIMOTO, S. & MATSUI, Y. (1975): Crystal structures of pyroxene-type $ZnSiO_3$ and $ZnMgSi_2O_6$. *Acta Cryst.* **B31**, 1041-1049.

NISHIZAWA, O. & AKIMOTO, S. (1973): Partition of magnesium and iron between olivine and spinel, and between pyroxene and spinel. *Contr. Mineral. Petrology* **41**, 217-230.

PAPIKE, J. J., PREWITT, C. T., SUENO, S. & CAMERON, M. (1973): Pyroxenes: comparisons of real and ideal structural topologies. *Z. Krist.* **138**, 254-273.

RUTSTEIN, M. S. & WHITE, W. B. (1971): Vibrational spectra of high-calcium pyroxenes and pyroxenoids. *Amer. Mineral.* **56**, 877-887.

SAXENA, S. K. & GHOSE, S. (1971): Mg^{2+}-Fe^{2+} order-disorder and the thermodynamics of the orthopyroxene crystalline solution. *Amer. Mineral.* **56**, 532-559.

SHANNON, R. D. (1974): Systematic studies of interatomic distances in oxides. *Proc. NATO Adv. Study Inst. on Petrophysics*, Newcastle-upon-Tyne, April 22-26.

——— (1976): Revised effective ionic radii and systematic studies of interatomic distances in halides and chalcogenides. *Acta Cryst.* **A32**, 751-767.

——— & CALVO, C. (1973a): Crystal structure of $LiVO_3$. *Can. J. Chem.* **51**, 265-273.

——— & ——— (1973b): Crystal structure of $Cu_5V_2O_{10}$. *Acta Cryst.* **B29**, 1338-1345.

SMYTH, J. R. (1973): An orthopyroxene structure up to 850°C. *Amer. Mineral.* **58**, 636-648.

——— (1974): Experimental study on the polymorphism of enstatite. *Amer. Mineral.* **59**, 345-352.

SNELLENBURG, J. W. (1974): Computer simulation of the distribution of octahedral cations in orthopyroxene. *Amer. Mineral.* **60**, 441-447.

STEPHENSON, D. A., SCLAR, C. B. & SMITH, J. V. (1966): Unit-cell volumes of synthetic orthoenstatite and low clinoenstatite. *Mineral. Mag.* **35**, 838-846.

SUENO, S., CAMERON, M. & PREWITT, C. T. (1976): Orthoferrosilite: high-temperature crystal chemistry. *Amer. Mineral.* **61**, 38-53.

TAKEDA, H. (1971): Silicon-aluminum substitution in some aluminum orthopyroxenes and micas. *Amer. Cryst. Assoc. Winter Meet. Program Abstr.*, 45.

——— (1972a): Tetrahedral sizes in orthopyroxenes and silicon-aluminum ordering. *Amer. Cryst. Assoc. Winter Meet. Program Abstr.*, 34.

——— (1972b): Crystallographic studies of coexisting aluminan orthopyroxene and augite of high-pressure origin. *J. Geophys. Res.* **77**, 5798-5811.

——— & RIDLEY, W. I. (1972): Crystallography and chemical trends of orthopyroxene-pigeonite from rock 14310 and coarse fine 12033. *Proc. Third. Lunar Sci. Conf., Geochim. Cosmochim. Acta, Suppl. 3, Vol.* **1**, 423-430.

THOMPSON, J. B. (1970): Geometrical possibilities for amphibole structures: model biopyriboles. *Amer. Mineral.* **55**, 292-293.

VANDER SANDE, J. B. & KOHLSTEDT, D. L. (1974): A high-resolution electron microscopy study of exsolution lamellae in enstatite. *Phil. Mag.* **29**, 1041-1049.

VIRGO, D. & HAFNER, S. S. (1969): Fe^{2+}, Mg order-disorder in heated orthopyroxenes. *Mineral. Soc. Amer. Spec. Pap.* **2**, 67-81.

——— & ——— (1970): Fe^{2+}-Mg order-disorder in natural orthopyroxenes. *Amer. Mineral.* **55**, 201-233.

WARREN, B. E. & MODELL, D. I. (1930): The structure of enstatite $MgSiO_3$. *Z. Krist.* **75**, 1-14.

WOOD, B. J. & BANNO, S. (1973): Garnet-orthopyroxene and orthopyroxene-clinopyroxene relationships in simple and complex systems. *Contr. Mineral. Petrology* **42**, 109-124.

ZACHARIASEN, W. H. (1968): Experimental tests of the general formula for the integrated intensity of a real crystal. *Acta. Cryst.* **A24**, 212-216.

Manuscript received April 1976, emended February 1977.